Isotopic evaluation of the National Water Model reveals missing agricultural irrigation contributions to streamflow across the western United States

Annie L. Putman[1], Patrick C. Longley[2], Morgan C. McDonnell[1], James Reddy[3], Michelle Katoski[4], Olivia L. Miller[1], and J. Renée Brooks[5]

[1]US Geological Survey Utah Water Science Center
[2]US Geological Survey Colorado Water Science Center
[3]US Geological Survey New York Water Science Center
[4]US Geological Survey Maryland-Delaware Water Science Center
[5]US Environmental Protection Agency, Pacific Ecological Systems Division

Correspondence: Annie L. Putman (aputman@usgs.gov)

Abstract. The National Water Model (NWM) provides critical analyses and projections of streamflow that support water management decisions. However, the NWM performs poorly in lower elevation rivers of the western United States (US). The accuracy of the NWM depends on the fidelity of the model inputs and the representation and calibration of model processes and water sources. To evaluate the NWM performance in the western US, we compared observations of river water isotope ratios ($^{18}O/^{16}O$ and $^2H/^1H$ expressed in δ notation) to NWM-flux-estimated (model) river reach isotope ratios. The modeled estimates were calculated from long term (2000-2019) mean summer (JJA) NWM hydrologic fluxes and gridded isotope ratios using a mass balance approach. The observational dataset comprised 4503 in-stream water isotope observations in 877 reaches across 5 basins. A simple regression between observed and modeled isotope ratios explained 57.9% ($\delta^{18}O$) and 67.1% (δ^2H) of variance, though observations were 0.5‰ ($\delta^{18}O$) and 4.8‰ (δ^2H) higher, on average, than mass balance estimates. The unexplained variance suggest that the NWM does not include all relevant water fluxes to rivers. To infer possible missing water fluxes, we evaluated patterns in observation-model differences using $\delta^{18}O_{diff}$ ($\delta^{18}O_{obs} - \delta^{18}O_{mod}$) and d_{diff} ($\delta^2H_{diff} - 8 * \delta^{18}O_{diff}$). We detected evidence of evaporation in observations but not model estimates (negative d_{diff} and positive $\delta^{18}O_{diff}$) at lower elevation, higher stream order, arid sites. The catchment actual evaporation to precipitation ratio, the fraction of streamflow estimated to be derived from agricultural irrigation, and whether a site was reservoir-affected were all significant predictors of d_{diff} in a linear mixed effects model, with up to 15.2% of variance explained by fixed effects. This finding is supported by seasonal patterns as well as groundwater levels and isotope ratios, and suggests the importance of including irrigation return flows to rivers, especially in lower elevation, higher stream order, arid rivers of the Western US.

1 Introduction

The western United States (US) is experiencing multidecadal drought (Williams et al., 2022) and declining streamflows (Milly and Dunne, 2020). Major rivers are running dry (Kornfield, 2022), lakes are shrinking (Ramirez, 2022; Fergus et al., 2020, 2022),

and water users are experiencing shortages and cuts (Bureau of Reclamation, Department of the Interior, 2022). These decreases in streamflow and groundwater fluxes are projected to continue in coming years (Miller et al., 2021a, b), with projected decreases in snowpack (Mote et al., 2021; Siirila-Woodburn et al., 2021) and increases in temperatures (Hicke et al., 2022). Under drought and snow drought stress, as well as changing wintertime precipitation patterns, river flows may become more difficult to forecast (Hammond and Kampf, 2020; Siirila-Woodburn et al., 2021). Yet, with decreasing water availability, water managers and other stakeholders tasked with managing and responding to current and future water supply increasingly depend on accurate streamflow predictions.

Fully routed, high spatial and temporal resolution streamflow models, like the National Oceanic and Atmospheric Administration's National Water Model (NWM) which is an application of the Weather Research and Forecasting (WRF) Hydro model (Gochis et al., 2018), provide short and medium term streamflow prediction in the United States, as well as analyses of past stream discharge at ungaged locations. The accurate, detailed, frequent results from the National Water Model may be used by emergency managers, reservoir operators, floodplain managers, and farmers to aid in water use decision making and flood or pollution risk evaluation. The accuracy of predictions and current snapshots produced by the model depend on 1) inclusion and faithful representation of relevant water sources and hydrologic processes 2) appropriate calibration of parameter estimations and 2) the fidelity of the model inputs.

With respect to the faithful representation of water sources, the major water sources to streams in the mountainous west include two broad water flux categories: runoff (also called quickflow, and may comprise surface or subsurface waters) and groundwater discharge (also called baseflow). Runoff during the summer comes from late season snowmelt, rain, and irrigation water. Groundwater discharge comes from shallow or deep in-ground water, typically recharged at high elevation by snowmelt. Rivers in the west derive the majority of their water from springtime melt of high elevation wintertime snowpack (Li et al., 2017; Hammond et al., 2023) and little water is contributed to streams at lower elevations where there is minimal snowpack (Miller et al., 2021b). Some of the melt water enters streams as surface runoff during late spring and summer, while the remainder recharges shallow and deep groundwater and later in the season or in subsequent years enters the stream as groundwater discharge (Barnhart et al., 2016; Miller et al., 2021a; Brooks et al., 2021; Wolf et al., 2023). Rain contributes runoff to streamflow, but even in areas receiving a substantial proportion of their total annual precipitation during summer in association with the North American Monsoon, only a small proportion of the total precipitation makes it to the stream (Solder and Beisner, 2020; Tulley-Cordova et al., 2021); most is evaporated from soils or transpired by plants (Milly and Dunne, 2020). Thus, lower elevation streams, particularly later in the summer, depend heavily on groundwater discharge from higher elevations to sustain their flows (Miller et al., 2016) and the majority of streams in lower elevation arid areas are likely to lose water to shallow groundwater recharge (Jasechko et al., 2021).

Within this hydrologic framework, human water use and management introduces complexity via reservoirs and managed release schedules, trans- and interbasin transfers, conveyances, and surface and groundwater withdrawals, as well as irrigation for agricultural crop or turf grass growth. Turf irrigation in cities composes the majority of household water use in most municipalities and agricultural irrigation can comprise up to 80% of total statewide water use in Western US states (Dieter et al., 2018). Water used for agricultural crop or turf grass growth locally intensifies water balance fluxes, through increases

in both water application and evapotranspiration in these select tracts of land. Depending on the method, both agriculture and turf grass irrigation can contribute to local groundwater recharge (Grafton et al., 2018), with greater recharge coming from flood irrigation compared to sprinkler or drip irrigation methods. Water for irrigation can come from either surface or groundwater withdrawals. The irrigation water source may have both direct and indirect influences on streamflows particularly during low flow seasons, and may, depending on conditions, may contribute to streamflow increases, decreases, or delays in discharge (Essaid and Caldwell, 2017; Condon and Maxwell, 2019; Ketchum et al., 2023). However, these processes and fluxes are not currently explicitly included in the NWM.

Past NWM evaluations have leveraged streamgage measurements (Hansen et al., 2019; Seo et al., 2021; Towler et al., 2023) and model evaluation using streamgage measurements is included in the NWM WRF-Hydro workflow (Gochis et al., 2018). Using measured discharge to evaluate the NWM is useful because the data are publicly available at high spatial and temporal resolution (e.g., dataset used in Towler et al. (2023)). However, evaluation of streamflows with measured discharge 1) may allow modelers to get the correct total streamflow values and temporal patterns at a reach for the wrong process reasons or 2) may suggest that the model could be improved due to mismatches between measured and modeled data, but cannot provide information on the specific process(es) or sources responsible for the errors.

Among the climatic regions covered by the NWM, model streamflow evaluation metrics perform the most poorly in the Western US in lower elevation reaches. Metrics like the Kling–Gupta efficiency (KGE) indicate pervasive mismatches between measured and modeled streamflows and percent bias (PBIAS) results showed that simulated streamflow volumes tend to be overestimated in the west (Towler et al., 2023). Similarly, Hansen et al. (2019) found that the NWM has difficulty estimating flows during drought or low flow years in the Colorado River Basin. In the low elevation stream reaches of the Western US, disagreement between the NWM flows and observations within anthropogenically-altered reaches may come from incomplete representation of anthropogenic water sources or processes in the NWM.

In the western US, low elevation waterways have moderate to high potential for anthropogenic alteration (Fergus et al., 2021). Rivers and surface water supplies are managed by dams, and a large proportion of total water use is allocated to irrigating agriculture (Dieter et al., 2018). However, the NWM does not explicitly include surface water removal for agricultural irrigation nor subsurface return flows from irrigation in its streamflow computations. Likewise, the NWM represents inflow and outflow of lakes and reservoirs as passive storage and releases, with no active reservoir management. Both of these omissions may be contributors to the large errors observed in the NWM in lower elevation areas where land use includes large amounts of along-river agriculture and streamflow is heavily managed through reservoir operations. Unfortunately, the effects of contributions of these two water sources on streamflow are difficult to identify and quantify through evaluations of streamflow records alone.

Elemental or isotope ratios in media associated with hydrologic processes (i.e., water, dissolved gasses, suspended sediments, dissolved ions) are used used to track the contributions of specific water sources (e.g., groundwater, runoff) to rivers or other surface waters (Cook and Solomon, 1995; Hall et al., 2016; Gabor et al., 2017). Tracers are useful because they provide information that is otherwise impossible to disentangle from direct measurements of streamflow.

Stable water isotopes (O and H) have been used to extract hydrologic process information (Jasechko et al., 2014; Evaristo et al., 2015) and diagnose process limitations in other modeling contexts (Nusbaumer et al., 2017; Putman et al., 2019). Water

comprises three commonly measured stable isotopologues: the most abundant, light atom-bearing $^{1}H_{2}^{16}O$, as well as heavy oxygen bearing ($^{1}H_{2}^{18}O$) and heavy hydrogen bearing ($^{1}H^{2}H^{16}O$) isotopologues. Measurements of stable water isotopes use the ratio of the heavy to light isotopologue for each atom ($R = {}^{18}O / {}^{16}O$ or $^{2}H / {}^{1}H$ and are expressed in delta notation ($\delta^{18}O$ and $\delta^{2}H$), where $\delta = 1000 * \left(\frac{R_{sample} - R_{standard}}{R_{standard}} \right)$). Samples with higher ratios may be described as 'enriched' with respect to an isotope relative to a reference, whereas those with lower ratios may be described as 'depleted' with respect to an isotope and relative to a reference.

The utility of any tracer comes from its spatial and temporal variability. In the case of water isotopes as tracers, variability arises from from isotopic fractionation, a physically-governed 'sorting' of heavy-atom bearing water molecules ($^{1}H_{2}^{18}O$ and $^{1}H^{2}H^{16}O$) from those bearing only light atoms ($^{1}H_{2}^{16}O$) that occurs during phase changes (i.e., evaporation, condensation, sublimation, deposition; Bowen et al., 2019). Spatial and temporal patterns of $\delta^{18}O$ and $\delta^{2}H$ are very similar, as evidenced by the strong correlations between $\delta^{18}O$ and $\delta^{2}H$ in precipitation (Craig, 1961; Putman et al., 2019) and in other waters, including those in the ground, surface, and soil (Evaristo et al., 2015; Tulley-Cordova et al., 2021).

Linear relationships between $\delta^{18}O$ and $\delta^{2}H$ in precipitation, and waters derived from precipitation (e.g., ground, river, lake, soil) are the basis for the ubiquitous water line (WL) framework, in which the best fit lines of the form $\delta^{2}H = \beta\delta^{18}O + I$ are calculated for different water types (e.g., meteoric (MWL), ground (GWL), surface (SWL)) and are defined either for specific points (local, e.g., LMWL) or for regional or global datasets (e.g., GMWL) comprising multiple points. Slopes and intercepts of these lines have useful physical interpretations (Putman et al., 2019), particularly as they relate to the global average conditions. Global average conditions are represented by the Global Meteoric Water Line (GMWL), which has a slope of 8 and intercept of 10. Differences between $\delta^{18}O$ and $\delta^{2}H$, relative to an expected, global average relationship are calculated using a secondary parameter called deuterium excess (defined as $d = \delta^{2}H - 8 * \delta^{18}O$). Deuterium excess ($d$) is used to detect evaporation of precipitation and surface waters, evaporation under a vapor pressure gradient or non-equilibrium condensation processes, like snow formation in mixed phase clouds or isotopic fractionation during the melting of snow (Ala-aho et al., 2017; Putman et al., 2019; Bowen et al., 2018; Sprenger et al., 2024).

Because hydrologic processes including groundwater recharge, discharge, and precipitation runoff do not cause isotopic fractionation, we can use water fluxes from hydrologic models with estimates of the isotope ratios of those fluxes on the appropriate timescales to produce river water isotope estimates. This works well because the groundwater and runoff fluxes to summertime streamflow in the Western US have distinct stable isotope ratios due to seasonal and spatial controls on precipitation isotope ratios. The signatures of groundwater inflow and snowmelt tend to have the lowest isotope ratios of the water sources in the hydrologic system and tend to be relatively temporally invariant (Bowen, 2008; Feng et al., 2009; Jasechko et al., 2014; Solder and Beisner, 2020; Tulley-Cordova et al., 2021). In contrast, summer precipitation, which contributes runoff to streams, tends to have higher isotope ratios than groundwater (Jasechko et al., 2014; Tulley-Cordova et al., 2021).

Anthropogenic modifiers of streamflow that are not included explicitly in the NWM (i.e., irrigation and reservoirs) may be expected to alter the isotopic signature of streamflow downstream of the river water source areas in the headwaters. Agricultural irrigation can contribute both runoff to streams and recharge groundwater (Essaid and Caldwell, 2017; Gochis et al., 2018). Evaporation occurring during conveyance and application increases the isotope ratios in water recharged by irrigation and

decreases d (Craig and Gordon, 1965; Yang et al., 2019). This isotopic signature is passed along to the plants (Oerter et al., 2017). Thus, irrigation-sourced recharge (runoff or ground) exhibits an evaporated isotopic signature that is distinct from naturally recharged groundwater or precipitation runoff. The effects of evaporation on the isotope ratios of the return flows are expected to be greater in arid areas with higher summer temperatures and higher vapor pressure deficits. Although lakes can be isotopically enriched with lower d (isotopically evapoconcentrated) relative to other surface waters (Bowen et al., 2018), we do not expect similar signals of evaporation-driven isotopic enrichment from reservoirs. Relative to natural lakes across the US, evaporation rates from western lakes are low relative to inflow (Brooks et al., 2014). Instead, reservoirs may alter the isotope ratios of streamflow through retention of and later discharge of spring snowmelt. Thus, reservoir outflow may have lower isotope ratios and higher d than the upstream rivers during the summer months.

In this study, we compared hydrologic model-informed estimates of long term mean streamflow isotope ratios with stream water isotope observations across the western US. The model-informed estimate of river water isotope ratios used an isotope mass balance methodology that combined the long term average water fluxes of the NWM and water stable isotope datasets. If the NWM constrains all water sources affecting streamflow, we expect the differences between the isotope mass balance results and isotopic observations (observation-model differences) will be small and be uniformly positive or negative throughout each basin. If we observe spatial and/or seasonal variability and structured patterns in observation-model differences within basins (i.e., patterns with elevation, stream order, or aridity), particularly with respect to the sign of the difference, we may infer that the NWM is incorrectly partitioning runoff and groundwater fluxes, or missing important water sources. We hypothesize that if we observe spatial variability and structured patterns in our observation-model difference data, we will observe higher isotope ratios and lower d in more arid reaches reflecting the influence of irrigation return flows, which we expect bear an isotopic signal of evaporation, on streamflow as compared to higher elevation, humid or seasonally snowy reaches with minimal anthropogenic influence.

2 Methods

This study analyzes spatial patterns in observation-model differences to evaluate missing sources of streamflow in the NWM in the western US. The 'model' estimates are produced using an isotope mass balance approach, where water fluxes were supplied by NWM simulations of groundwater and surface runoff fluxes (National Oceanographic and Atmospheric Administration, 2022) and isotope ratios came from gridded groundwater and precipitation stable isotope products (Bowen (2022b); Bowen et al. (2022), Figure 1, Section 2.3). These mass balance estimates were compared to a large collection of stable river water isotope observations, and both the compiled observations and mass balance estimates are publicly available (Reddy et al. (2023), Figure 1, Section 2.4). Differences between observations and modeled data were compared in an error-partitioning framework (Section 2.5), and we tested the hypothesis that spatial variability in observation-model differences contains a signature of agricultural water use (Section 2.6). A groundwater isotope ratio dataset and a well water surface elevation relative to river surface elevation dataset from Jasechko et al. (2021) were used as independent lines of evidence supporting our analysis of observation- mass balance estimate differences (Section 2.7).
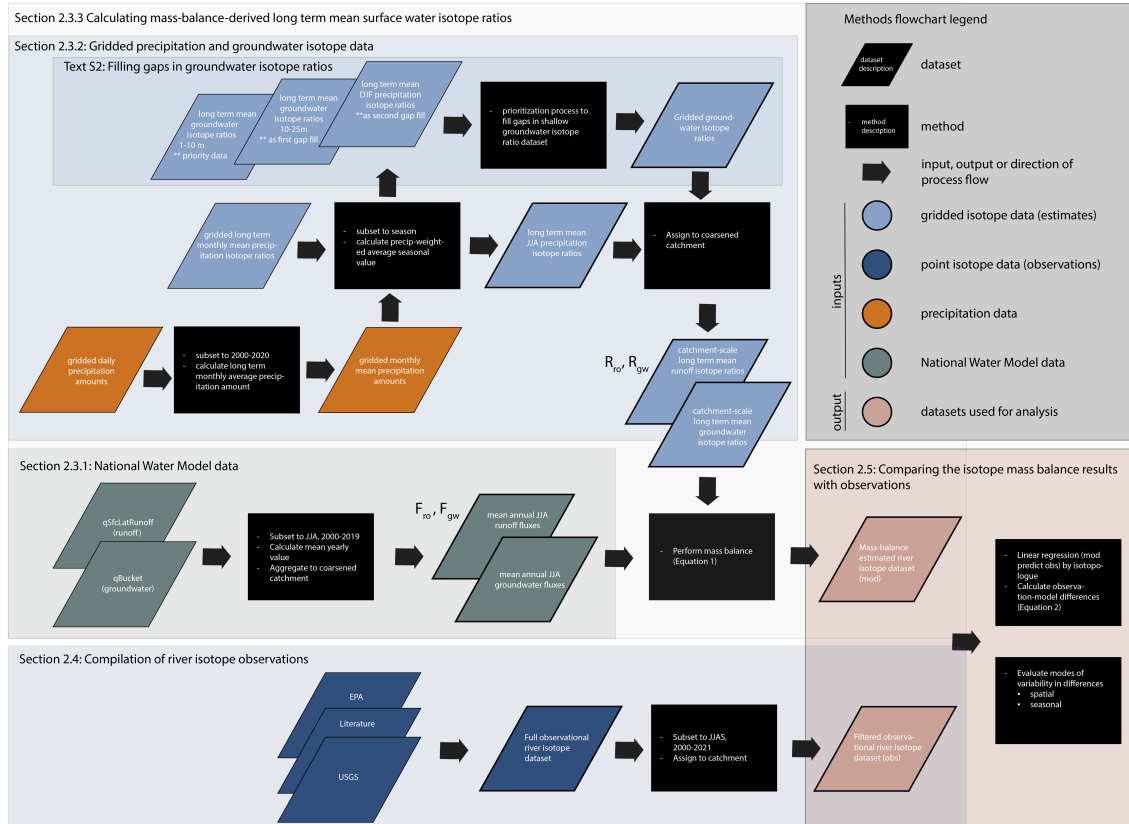
Figure 1. Diagram showing methods and datasets as described in Sections 2.4-2.6. Four datastreams were used to formulate the long isotope mass balance estimates of river isotope ratios: gridded precipitation isotope estimates (Bowen, 2022b), gridded groundwater isotope estimates (Bowen et al., 2022), gridded precipitation data (University of East Anglia Climatic Research Unit and Harris, I.C. and Jones, P.D. and Osborn, T. , 2021) and NWM data (National Oceanographic and Atmospheric Administration, 2022) . Three data categories contributed to the observational river isotope dataset: USGS (U.S. Geological Survey, 2022), EPA (U.S. Environmental Protection Agency, 2016b, 2020), and literature datasets accessed from the Water Isotopes database (Putman and Bowen, 2019).

2.1 Temporal domain

Our analysis was constrained to summer months (June, July, August) between 2000 and 2019. The specific months chosen reflect those with greatest evapotranspiration and thus consumptive water use and correspond to the season with the largest number of spatially distributed river water isotope observations.

2.2 Spatial domain

We selected 5 hydrologic unit 2-digit code (HUC2) scale basins (U.S. Geological Survey, National Geospatial Technical Operations Center, 2023) in the Western US to compose our study area: the Upper Colorado (14), Lower Colorado (15), Great Basin (16), Pacific Northwest (17), and California (18). All basins were characterized by rivers sustained by wintertime snowpack mediated by groundwater infiltration and discharge. All basins also included water management through impounds and substantial water use for agriculture. In a simplified Köppen climate classification (Rubel and Kottek, 2010), the southern and central portions of the study area were characterized as arid, whereas much of the northern and mountainous portions of the study area was classified as warm temperate or seasonally snowy.

The spatial domain and streamflow routing were represented by a network of flowlines (reaches) and catchments (n=15787, 1:1 flowlines:catchments) derived from the National Hydrography Dataset Plus (NHDPlus, (U.S. Geological Survey, 2019), see Text S1 for network processing details) and clipped to the spatial domain of our study. Catchments had a median size of 51 km^2 and a mean size of 221 km^2, and flowlines had a median length of 20 km^2 and a mean length of 32 km^2. All data used in this analysis were spatially joined to this network, and we retained attributes provided by NHDPlus for analysis, including catchment area, Strahler stream order, reach length, minimum and maximum catchment elevation, and feature code, which denoted the flowline path type.

2.3 Using isotope mass balance to estimate long term mean river isotope ratios

Using estimates of long term mean groundwater and precipitation isotope ratios (Bowen et al., 2022; Bowen, 2022b), we applied an isotope mass-balance to the NWM groundwater and surface runoff fluxes to streams (Figure 1). The operational hydrologic model is based on the open-source, community hydrologic model WRF-Hydro (Gochis et al., 2020a, b) and simulates and forecasts major water components (e.g., evapotranspiration, snow, soil moisture, groundwater, surface inundation, reservoirs, and streamflow) in real time across the CONUS, Hawaii, Puerto Rico, and the US Virgin Islands. In the NWM framework, surface and soil evaporation are wrapped into the evapotranspiration flux variable, and direct evaporation from rivers and reservoirs are not considered in the NWM surface water balance. Thus, we did not apply any additional isotopic fractionation to the groundwater and surface runoff isotopic fluxes. This approach produced an estimated long term mean isotope ratio for river reaches in the western US. These estimates were directly comparable to river water isotope observations.

2.3.1   National Water Model data

We accessed lateral surface runoff (NWM variable qSfcLatRunoff, m^3 s^{-1}) and groundwater (qBucket, m^3 s^{-1}) fluxes from
the NWM v 2.1 Analysis Assimilation dataset (National Oceanographic and Atmospheric Administration, 2022) for our mass
balance estimates (Figure 1). The NWM runoff term (qSfcLatRunoff) only includes surface runoff and does not include subsur-
face runoff. Instead, subsurface runoff is routed from the bottom of the soil layer to the groundwater bucket (qBtmVertRunoff).
We also accessed streamflow (streamflow, m^3 s^{-1}) fluxes as a reach scale quantity to be included in the analyses of results. All
NWM variables we used are available at the NHDPlus reach scale on an hourly timestep between 2000 and 2019. We subset
these variables to the summer months (June, July, and August) and calculated the mean water fluxes to each reach for the
summer season of each year. The interannual variability in the summer fluxes was leveraged as an estimate of the uncertainty
of the long term mean summer water fluxes.

2.3.2   Gridded precipitation and groundwater isotope data

The precipitation and groundwater stable isotope ratios (δ^2H, δ^{18}O) that we used to perform the isotope mass balance came
from two publicly available gridded products. Both represent long term means or climatologies and provide estimates of
uncertainty.

We obtained monthly precipitation isotope ratio climatological predictions and uncertainty estimates (1 standard deviation)
for both H and O from Bowen (2022b). The monthly USA grids were available at 1 km, and were produced with the OIPC
v3.2 database (Bowen, 2022a) following methods described in Bowen et al. (2005). Monthly grids have been adjusted for
consistency with annual values (see version notes for OIPC2.0; Bowen, 2006). In general, isoscape accuracy depends on
the spatial and temporal coverage of point datasets available to produce the isoscape. The Bowen (2022b) product is the
highest resolution gridded product available for the conterminous United States, and in contrast to other global or regional
gridded isotope products, is produced using precipitation isotope ratio data from not only the Global Network of Isotopes in
Precipitation (GNIP), but also the US Network of Isotopes in Precipitation, and a host of other precipitation samples collected
and stored in the Water Isotopes Database (Putman and Bowen, 2019). In our input dataset, the median standard deviations
of both δ^2H and $\delta^{18}O$ are about 0.12‰, but may be as large as 2-3‰, depending on the region and isotope, based on a N-1
jacknife approach to error estimation (Bowen and Revenaugh, 2003).

We calculated the precipitation-weighted long term mean summer (June, July, August) and winter (December, January,
February) seasonal isotope ratio climatologies with long term monthly mean precipitation climatologies calculated from the
Climatic Research Unit (CRU) mean monthly precipitation amounts (Harris et al., 2020; University of East Anglia Climatic
Research Unit and Harris, I.C. and Jones, P.D. and Osborn, T. , 2021) for the period 2000-2020. The precipitation weighted
mean seasonal climatology error was calculated analytically from the timeseries.

The groundwater isoscapes used in this analysis were produced by Bowen et al. (2022) for 7 depth intervals ranging from 1
to 1000m. The groundwater isoscapes were not temporally resolved. The authors report errors smaller than 0.71 and 1.07‰ in
$\delta^{18}O$ and δ^2H estimates, respectively, based on a cross-validation approach. The approach was validated using an independent

dataset and found that variance in the modeled groundwater predicts 92% of the variance in the validation dataset, with no bias. The authors suggest that because the approach estimates groundwater isoscapes at different depth intervals it produces more accurate estimates than methods for producing bulk groundwater isoscapes.

Because this project focuses on groundwater discharge to streams, we preferentially utilized the 1-10m depth interval. However, this layer contained some data gaps where insufficient well data were present to perform an estimate. Where available, we filled these data gaps using either other groundwater depths or mean winter precipitation (DJF) as described in Text S2. The groundwater isotope ratio data included estimates of uncertainty, which were retained for the characterization of uncertainty around the mass balance isotope ratio estimates.

The gridded precipitation and groundwater isotope datasets and their uncertainties were assimilated to the NHDPlus spatial framework. Because the raster data grid sizes were larger than the catchment sizes we employed a distance minimization approach using the centroid of the catchment and the centroids of the grid cells.

2.3.3 Calculating mass-balance-derived long term mean surface water isotope ratios

To estimate the long term mean surface water isotope ratio ($R_{sw,r}$) at each reach (r) in the spatial domain (Equation 1), we accumulated the groundwater (gw) and surface runoff (ro) isotope fluxes (i.e., the isotope ratio multiplied by the water flux, $R * F$) for all reaches (i) from the headwaters downstream to the reach. The isotope ratio for surface runoff (R_{ro}) came from the summer mean gridded precipitation isotope ratios and the isotope ratio for the groundwater flux (R_{gw}) came from the gridded groundwater isotope ratios (see Section 2.3.2). The summed isotope fluxes were divided by the summed surface runoff and groundwater fluxes.

$$R_{sw,r} = \frac{\sum_{i=0}^{r} R_{gw,i} * F_{gw,i} + R_{ro,i} * F_{ro,i}}{\sum_{i=0}^{r} F_{gw,i} + F_{ro,i}} \tag{1}$$

Our long term mean estimates of $R_{sw,r}$ are subject to uncertainty from 1) internannual variations in the mean summer volumetric contributions of groundwater and surface runoff to streamflow and 2) because the long term mean estimates of the groundwater and precipitation isotope ratios are subject to uncertainty arising from underlying data coverage as well as interannual variability. To constrain uncertainty in our long term mean estimates of $R_{sw,r}$, we calculated 200 estimates of R_{sw} per reach by taking 10 random draws of from the isotope ratio distributions (assuming a normal distribution), for each of the 20 years of record. This approach uses interannual variability in surface runoff and groundwater fluxes to constrain the variability in the water flux component of the calculation, and uncertainty in the isotope ratio estimates to constrain the uncertainty in the isotope ratio component of the calculation. Joint distributions (of either H and O, or isotopes with water fluxes), were not used because information about how the isotope ratios might covary was not available from the gridded isotope datasets and no assumptions were made about how the isotopes might vary with interannual variability in climatic conditions. Similarly, no assumptions were made that the precipitation and groundwater isotope ratios covaried in time. These 200 estimates were used to calculate a long-term mean estimated isotope ratio for river water in each reach of the network and to evaluate uncertainty in our estimates.

2.4 Compilation of river isotope observations

The results of the mass balance calculations were compared with observations of stable water isotope ratios from rivers collected between 2000 and 2021, during the growing season months of June, July, August and September. We included two additional years (2020 and 2021) as well as data from the month of September beyond the temporal constrains of the NWM model domain in our set of observations. This decision was made to maximize the amount of data and number of unique river reaches in the spatial domain that are available for analysis, and reflects the assumption that the long term mean river isotope ratios calculated from the mass balance approach will be insensitive to inclusion or exclusion of a small number of additional years or an additional growing season month.

We compiled surface water stable isotope (δ^2H, δ^{18}O) measurements from various sources including the Environmental Protection Agency (EPA), the United States Geological Survey (USGS) National Water Information System (NWIS, U.S. Geological Survey (2022)), and published datasets assimilated in the Water Isotopes Database (Putman and Bowen, 2019). Not all reaches had one or more stable water isotope observations, and river reaches with multiple stable water isotope ratio observations were sometimes, but not always, from the same sampling site within the catchment.

The EPA surface water stable isotope data came from the National Rivers and Streams Assessments (NRSA, U.S. Environmental Protection Agency (2016b, 2020)) and the National Lakes Assessment (NLA, U.S. Environmental Protection Agency (2009, 2016a)). These data were collected once or twice per summer on a five year rotating basis as part of routine sampling campaigns. Over the time period of our analysis, we obtained three collections of NRSA samples (2008-2009, 2013-2014, and 2018-2019). Sites were sometimes but not always resampled among the campaigns. Sampling was stratified based on Strahler stream order and by state ensuring that all orders were sampled within each state in the assessments (U.S. Environmental Protection Agency, 2016b, 2020). This means that higher order reaches are less frequently sampled than medium or low order reaches.

The USGS surface water stable isotope data for rivers were downloaded through the NWIS API (U.S. Geological Survey, 2022) and the literature data came from published and unpublished sources that are publicly available through the Water Isotopes Database (Putman and Bowen, 2019). Stable isotope collections are not part of routine measurements for the USGS, but rather are collected by specific USGS projects. Thus, stable isotope data collections from the USGS and literature datasets tended to be spatially and temporally clustered.

2.5 Comparing the isotope mass balance results with observations

The relationship of the NWM isotope mass balance (modeled) to the river isotope observations were evaluated using correlation and simple regression analyses, where the modeled isotope ratio (either δ^2H or $\delta^{18}O$) values are used to predict the observed isotope ratios. We evaluated the results with all unaveraged observations and mean isotope ratio at river reaches with multiple observations. A Pearson correlation analysis was performed using the 'corr()' function of python's 'pandas' package (Wes McKinney, 2010; The pandas development team, 2020). Regression analysis was performed using the ordinary least squares (OLS) function in the python 'statsmodels' package (Seabold and Perktold, 2010).

We calculated the likelihood that an observation and the model result came from the same distribution, based on the variance in the model estimate, and variance associated with river water isotope observations (Text S3) using a two-tailed t-test. We reported p-values, where p<0.1 indicated that the isotope mass balance estimate was statistically different from the observed surface water isotope ratio for the specific element (H or O).

2.5.1 Calculating observation-model differences

We calculated the observation (*obs*)-model estimate (*mod*) differences in both $\delta^{18}O$ and δ^2H, by subtracting the model estimate from the observation ($\delta^{18}O_{diff} = \delta^{18}O_{obs} - \delta^{18}O_{mod}$; $\delta^2H_{diff} = \delta^2H_{obs} - \delta^2H_{mod}$). Using both isotope systems, we established a framework for interpretation of our results (Figure 2) that utilizes movement along or deviation from the global mean $\delta^2H : \delta^{18}O$ ratio of 8 that is used to represent fractionation that occurs at equilibrium and defines the slope of the Global Meteoric Water Line (GMWL, Craig, 1961).

Observation-model differences may arise from either 1) incorrect model source representation (i.e., missing water sources or incorrect fluxes of established sources) or 2) errors in the isotope ratio datasets used for the isotope mass balance calculation. Thus, for positive or negative values of $\delta^{18}O_{diff}$ and δ^2H_{diff} that exhibit a $\delta^2H_{diff} : \delta^{18}O_{diff}$ ratio of 8, we infer either errors in NWM with respect to the proportions of surface runoff and groundwater contributed, or errors in the gridded isotope ratios (likely groundwater, due to its disproportionate contributions to streamflow). For positive or negative $\delta^{18}O_{diff}$ and δ^2H_{diff} with $\delta^2H_{diff} : \delta^{18}O_{diff}$ ratios different from 8, we infer that the NWM is missing uncharacterized water sources with isotope values bearing a signature of non-equilibrium fractionation. We quantify differences of $\delta^2H_{diff} : \delta^{18}O_{diff}$ ratios from 8 using a metric of similar to d (Equation 2).

$$d_{diff} = \delta^2H_{diff} - 8 * \delta^{18}O_{diff} \tag{2}$$

We can interpret combinations of $\delta^{18}O_{diff}$ and d_{diff} together, as well as d_{diff} independently to infer the uncharacterized sources responsible for the observation-model difference. This framework is useful because the ratios of δ^2H to $\delta^{18}O$ of the isotopic inputs to the isotope mass balance tend to be close to 8 (Bowen, 2022b; Bowen et al., 2022) whereas those from the observations more often differ from 8 (U.S. Environmental Protection Agency, 2016b, 2020). This means that all non-zero d_{diff} values can be used to identify omitted water sources with non-equilibrium fractionation signals and can be used to diagnose where these sources may contribute to streamflow. The conditions of this study, based on the data and approach, mean that the mass balance approach represents a null hypothesis that all processes and sources contributing to streamflow carry an isotopic signal of equilibrium fractionation (i.e., precipitation, groundwater, routing). In other instances, where the modeled approach could reflect a combination of equilibrium and non-equilibrium processes, the interpretation of observation-model differences, particularly in terms of the d_{diff} axis, may change.
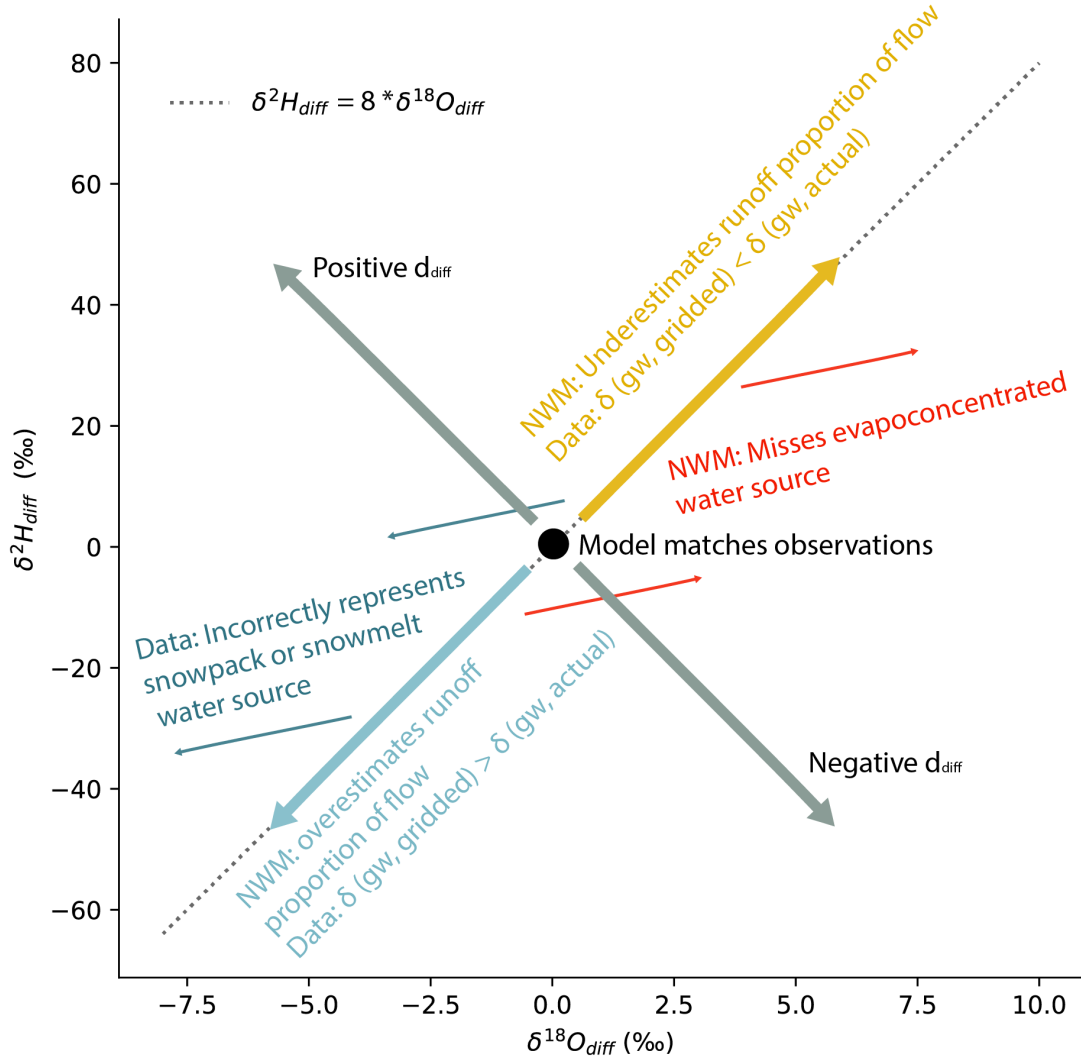
Figure 2. Schematic for interpretations of observation model differences utilizing dual isotope difference space and assumptions about the expected relationships between $\delta^{18}O_{diff}$ and $\delta^2 H_{diff}$. The annotations associated with 'NWM' specify the sort of hydrologic model error (i.e. water source apportionment) that could produce the observation-model comparison result, if all isotope data supplied to the isotope mass balance are correct. The annotations associated with 'Data' specify the sort of error in the gridded isotope datasets that could produce the observation-model result if all NWM water source contributions are assumed to be correct. The interpretations of the secondary mode of variability, captured by d_{diff}, depend on the 'model' producing results that reflect equilibrium relationships between $\delta^{18}O$ and $\delta^2 H$.

2.6 Evaluating variability in observation-model differences

Following the spatial strength of our dataset, which relies heavily on the EPA NRSA datasets, we focused on evaluation of spatial variability in observation-model differences in our dataset. We evaluated temporal variability to 1) support findings from our analysis of spatial variability and 2) determine whether there may be spatial-temporal covariance which influences our results.

Spatial structure in the observation-model differences were evaluated graphically by comparison of $\delta^{18}O_{diff}$ and d_{diff} with catchment mean elevation, Strahler stream order, and Köppen climate class (Rubel and Kottek, 2010). The former two variables were retained from the NHDPlus catchment dataset (U.S. Geological Survey, 2019). The former was joined to the spatial framework as described in Text S4.

Spatial structure in the observation-model differences were evaluated statistically with linear mixed effects modeling using the basin (HUC2) as a random variable using the python 'statsmodels' module and the 'mixedlm()' function (Seabold and Perktold, 2010). Linear mixed effects modeling with basin as the random (grouping) variable was selected for the analysis method because water in streams at low elevations is likely to be more isotopically similar to water in the basin headwaters than a nearby stream in a different basin with different water source regions. Thus, we assume the groups are likely to have different mean values reflecting their hydrologic and climatic differences. Although we also expect that the relationship of the response variable d_{diff} to the explanatory variables may differ among basins, both our response and explanatory variables contain substantial scatter as well as small numbers of high leverage points in each basin, such that a more nuanced analysis that includes temporal aspects of variability would be likely to produce misleading results.

Using the linear mixed effects approach, we tested the statistical relationship between d_{diff} and the ratio of actual evaporation to precipitation ($\frac{ET_a}{P}$, Text S4), catchment mean elevation, fraction of streamflow estimated to come from agricultural return flows (Text S5), and a categorical variable indicating influence of large reservoirs (capacity >50,000 acre-feet, Text S5.2). We performed statistical analysis on all streams not categorized as intermittent, ditches, or canals.

To assess how the observation-model difference may change over the growing season, in which the relative fraction of agricultural water in a waterway may increase due to low flows and increased water use, we obtained all sites-year combinations where there were at least three observations during at least three of the four months (Jun-Sep) of the growing season. We required one of the months be the month of June. From the June value(s) of $\delta^{18}O_{diff}$ and d_{diff} for a site-year combination, we subtracted the $\delta^{18}O_{diff}$ and d_{diff} values calculated for other months at the same site and from the same year. We evaluated the distribution of the aggregate results, as well as the distributions at the HUC2 basin scale by comparing their means and interquantile ranges.

Interannual variability was also assessed (Text S6) to ensure that patterns in the other modes of variability did not arise due to either covariability in spatial and temporal patterns of sampling, or the timescale difference between our isotope mass balance estimates (long term mean) and observations (instantaneous).

2.7 Evaluation of independent lines of evidence supporting signature of agricultural water use in rivers

Because it is difficult to disentangle the effects of elevation and aridity from the effects of human water use and management due to their spatial covariance, we utilized analyses of independent datasets to support the results of our statistical inference. The analyses evaluated relationships between land use or cover and groundwater isotope ratios and the fraction of well water levels that are below the nearby river level in catchments across the western US.

2.7.1 Associating groundwater stable isotope observations with land use / land cover types

Estimates of the isotopic evapoconcentration of groundwater associated with different land use and land cover classes supports our inferences from observation-model differences. We made the associations between groundwater isotope ratios and land use classes at a HUC12 scale (U.S. Geological Survey, National Geospatial Technical Operations Center, 2023).

We considered five land use type categories that were aggregations of two or more National Land Cover Database (Dewitz and U.S. Geological Survey, 2021) categories. The 'desert' category was composed of barren land (NLCD code=31), shrub/scrub (52), and grasslands/herbaceous (71) land classes. The 'forest' category was composed of evergreen, deciduous and mixed forests (41-43). The 'developed' category was composed of all the 'developed' classes, including open (21-24). The 'agriculture' category was composed of pasture/hay (81) and cultivated crops (82). The final category, 'water and wetlands' included all other land types, which include open water (11), perennial ice/snow (12), woody wetlands (90) and emergent herbaceous wetlands (95). We assigned the dominant land use/land cover category for each HUC12 using data based on the land use type with the greatest fractional coverage.

We compiled groundwater stable isotope ($\delta^{18}O$, $\delta^2 H$) measurements from the USGS NWIS (U.S. Geological Survey, 2022), and published datasets assimilated in the Water Isotopes Database (Putman and Bowen, 2019). The groundwater isotope ratio observations were spatially joined to the hydrologic units. We did not place temporal or well depth constraints on the samples used in our analysis. Not imposing well depth constraints may contribute to scatter associated with differences in water sources recharging shallow groundwater compared to deeper confined aquifers.

2.7.2 Evaluation of NWM groundwater discharge with well level fractions

The Jasechko et al. (2021) dataset compared river surface elevations with river-side well water elevations within catchments. The approach produced the fraction of wells in a catchment whose water surface levels were lower than the water surface level of the nearby river. In catchments where most well water levels are below the river water level (scores close to 1), we expect the river to lose water to shallow groundwater recharge under the right geologic conditions (e.g., permeability). In contrast, in catchments where most well water levels are above the river water level (scores close to 0), we expect groundwater discharge to streams.

We predicted the long term mean summer NWM 'qBucket' magnitude using the Jasechko et al. (2021) dataset using a simple linear regression. This approach tests the hypothesis that if NWM accurately represents groundwater discharge to streams, the relationship of well water elevations to river surface elevation would predict the summer mean NWM groundwater discharge

flux (assuming a linear relationship between the two quantities), with some scatter to account for subsurface permeability and spatial variability in groundwater discharge rates. We then evaluated the effect of agricultural irrigation in a catchment on the relationship between NWM 'qBucket' (binned by to the 0-20th, 20th-40th, 40th-60th, 60th-80th, and 80th-100th percentiles) and the Jasechko et al. (2021) dataset. The evaluation was split into reaches influenced by irrigation sourced from groundwater and irrigation sourced from surface water, as well as reaches uninfluenced by irrigation water. Irrigation contributions and irrigation water sources were determined using the methods for estimating irrigation water use described in Text S5.1 and used elsewhere in our analysis.

3 Results and discussion

3.1 Evaluation of the isotope mass balance approach for estimating surface water isotope ratios

Our analysis evaluated 4503 stream stable isotope observations in 877 unique river reaches across the western United States relative to NWM-driven isotope mass-balance-derived estimates (hereafter, 'modeled') of the river isotope ratios. Of these, 448 reaches had more than one observation (often all at the same sampling site in the catchment, but sometimes at multiple sites, Figure S1), and up to 571 observations in a catchment (Figure S1 and S2). On average, across all data, the observations were significantly greater than the modeled values by 0.537 ± 0.033 ‰ and 4.81 ± 0.222 ‰ for $\delta^{18}O$ and $\delta^{2}H$, respectively (Figure 3). For $\delta^{18}O$ we observed a standard deviation of 3.16‰ for the observed data and 2.96‰ for the modeled data (for all data averaged by catchment). For $\delta^{2}H$ we observed a sample standard deviation of 25.4‰ for the observed data and 24.4‰ for the modeled data (for all data averaged by catchment, Figure 3).

We calculated surface water lines (SWL) for both the modeled and observed results using all available data (Figure 3). The observations yielded a SWL with a slope of 7.570 ($\pm$ 0.023), and intercept of 1.2301 ($\pm$ 0.320), which was significantly different from the slope of the GMWL slope of 8 and intercept of 10 and was within the range of local MWLs (LMWL) slopes for western North America (6.5-8) (Putman et al., 2019), reported in Table 1. The model results yielded a surface water line with a slope of 8.12 ($\pm$0.010) and an intercept of 8.06 ($\pm$ 0.14) which was more similar to, but still statistically different from the GMWL and differed from LMWLs for the region (Table 1). Comparison of the observation and modeled data distributions and water lines reveals evidence for evaporation of surface waters in the observations but not in the isotope mass balance results (Figure 3). This is because the primary source of streamflow in the modeling framework, high elevation groundwater discharge, does not bear an evapoconcentrated isotopic signature in our input dataset, and lower elevation water sources (groundwater or surface runoff) that could bear an isotopic signature of evaporation, depending on the region, are considered by the model to be minor contributors to streamflow over the timescale integrated by our study.

Despite the differences in the data distributions, the modeled isotope ratios and observed isotope ratios were well correlated (Table 2, Figures S4-7), with correlation coefficients between 0.761 and 0.866, depending on the isotopologue and whether individual observations or catchment means were considered. These correlations translated to statistically significant simple linear regressions where the modeled isotope ratios were used to explain the observed isotope ratios (Table 2). Depending on the isotopologue and whether individual observations or means were considered, the models explained between $\sim$ 58% and 75%
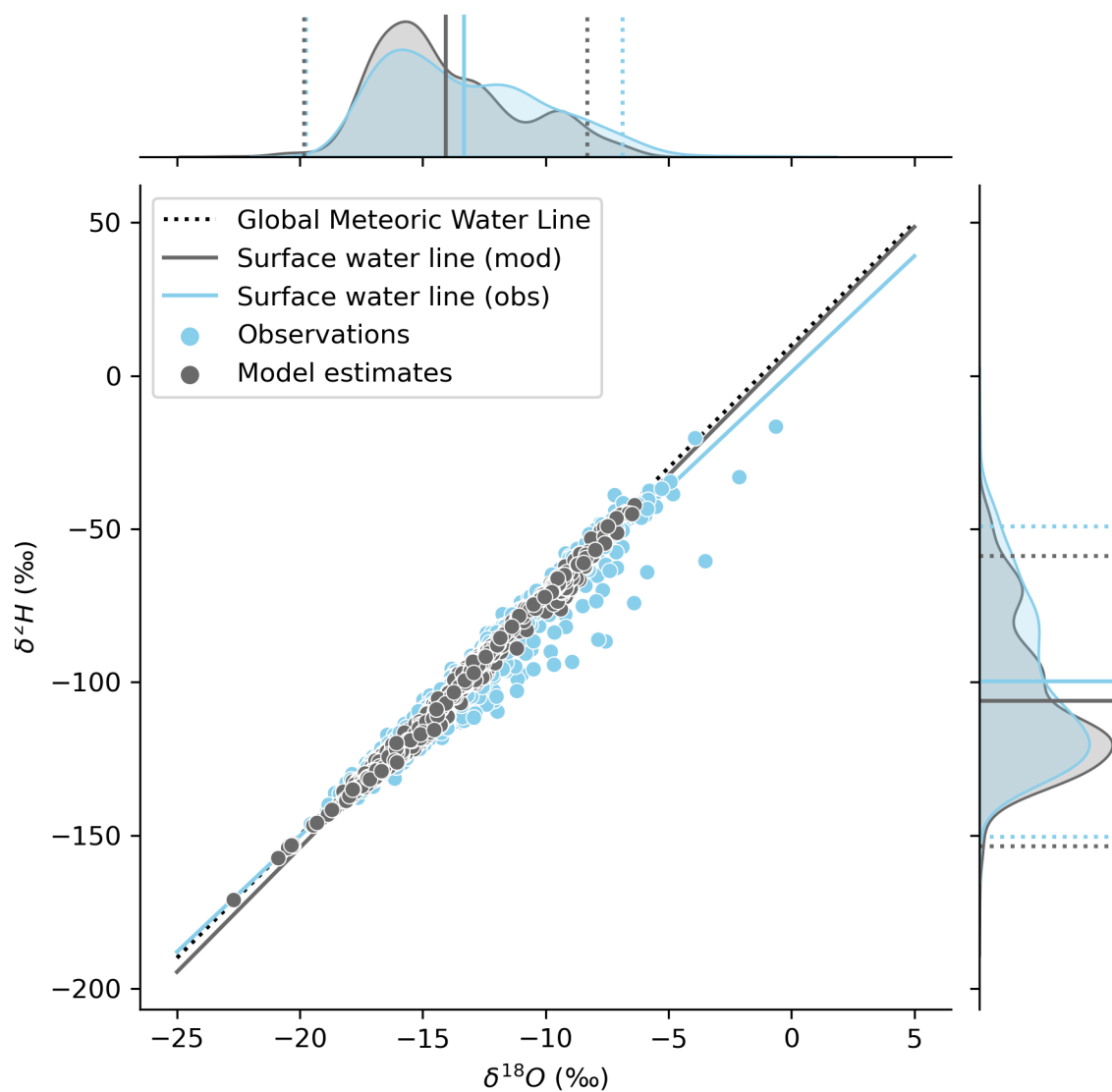
Figure 3. The distribution of the catchment mean observation (obs, blue) and isotope mass balance estimates (mod, gray) (n=448) with the Global Meteoric Water line (dotted) and the two datasets' surface water lines (solid lines). See Table 1 for water line statistics. Data distributions, including mean and two standard deviations of each data type (dotted lines), are shown in the plot margins. Observations plotting below the GMWL indicate evaporation, while those plotting above the GMWL may indicate mixed phase cloud processes or other non-equilibrium condensation processes (Putman et al., 2019).

Surface water lines:	β ($\pm$ s.e.)	I ($\pm$ s.e.)	R^2
Model-derived	8.12 ($\pm$ 0.010)	8.06 ($\pm$ 0.14)	99.3%
Observations	7.57 ($\pm$ 0.02)	1.23 ($\pm$0.32)	96.1%
Meteoric water lines:	β_{min}, β_{max} (β_{avg})	I_{min}, I_{max} (I_{avg})	
Global Meteoric Water Line	8	10	
Arid and Temperate dry summer LMWLs	6.56, 8.02 (7.57)	-10.5, 9.85 (3.02)	
Temperate humid and Continental LMWLs	7.34, 7.64 (7.49)	-3.82, 3.31 (0.62)	

Table 1. Surface water line slopes and intercepts ($\delta^2 H = \delta^{18}O + I$) compared to the Global Meteoric Water Line and published precipitation water line ranges (LMWLs) from different climate classifications in North America (data from Putman et al. (2019)). Because all regressions are highly significant, no p-values are shown.

Statistical model	n	Corr. coef	β ($\pm$ s.e.)	I ($\pm$ s.e.)	R^2
$\delta^{18}O_{obs} \sim \delta 18 O_{mod} + I$	4503	0.761	0.917 ($\pm$ 0.012)*	-0.645 ($\pm$ 0.168)*	57.9%
$\delta^{18}O_{obs,avg} \sim \delta^{18}O_{mod,avg} + I$	448	0.820	0.879 ($\pm$ 0.029)*	-0.891 ($\pm$ 0.414)*	67.3%
$\delta^2 H_{obs} \sim \delta^2 H_{mod} + I$	4503	0.819	0.937 ($\pm$ 0.010)*	-1.90 ($\pm$ 1.06)*	67.1%
$\delta^2 H_{obs,avg} \sim \delta^2 H_{mod,avg} + I$	448	0.866	0.905 ($\pm$ 0.025)*	-3.10 ($\pm$ 2.66)	75.1%
$\delta^2 H_{diff} \sim \delta^{18}O_{diff} + I$	4503	0.959	6.54 ($\pm$ 0.029)*	1.30 ($\pm$ 0.065)*	91.9%
$\delta^2 H_{avg,diff} \sim \delta^{18}O_{avg,diff} + I$	448	0.958	6.70 ($\pm$ 0.094)*	1.46 ($\pm$ 0.190)*	91.9%

Table 2. Correlation and regression results for observation-model comparisons. Regressions were performed on all data (n = 4503), as well as on the mean values in a subset of the reaches with more than one observation (n=448). An asterisk (*) indicates the coefficient is significant at p<0.1.

of the variance in the observations. The model explained more variance for $\delta^2 H$ than $\delta^{18}O$, and more variance for catchment mean values relative to individual observations. For all regressions, the slopes ranged from 0.879 to 0.937, with catchment mean slopes tending to be lower than slopes calculated from all observations. Intercepts for all regressions were close to, but less than 0, with lower intercepts associated with regressions calculated from catchment mean values, relative to regressions calculated from all observations. The statistically significant slopes of less than 1 and statistically significant intercepts arise in all observation-model comparison regressions because the observations tended to exhibit higher isotope ratios than the model estimated at the lower end of the isotopic distribution (Figures S4-7). Many of the catchments characterized by this pattern were in arid regions. The greater variance explained by the regressions using catchment means relative to the individual observations suggest that using a time varying inputs rather than calculating a long term mean river isotope ratio may further improve observation-model comparisons.

3.2 Model-observation differences

Of 4503 observations, 1763 $\delta^{18}O$ and 3306 $\delta^2 H$ observations were significantly different from the long term mean isotope mass balance NWM estimate at p<0.1. Of these, 1756 observations indicated significant differences for both $\delta^{18}O$ and $\delta^2 H$. This corresponded to a median absolute difference of 2.2‰ for $\delta^{18}O$ and 9.7‰ for $\delta^2 H$. For both, a larger proportion of the distribution indicated positive significant differences and those differences tended to be greater in absolute magnitude than the negative significant differences.

We used an observation-model difference interpretation framework (Figure 2) to gain process information that can be used to improve our understanding of terrestrial water balance and process inclusion in the NWM. The observation-model differences in $\delta^{18}O$ and $\delta^2 H$ were correlated (Figure 4) and yielded similar results for analyses performed with all data as compared to means of reaches with multiple observations (Table 2). Simple linear regressions, where variance in $\delta^{18}O_{diff}$ explained variance in $\delta^2 H_{diff}$, with all data and catchment mean data both explained about 92% of the variance, were significant and exhibited slopes of less than 8 (Table 2), suggesting the presence of errors arising from NWM omission of water sources that bear signatures of non-equilibrium processes.

In our dataset, model estimates do not deviate much from the GMWL, and deviate less than the observations (Figure 3). The model estimates reflect an assumption that water sources contributing to streamflow were subject only to equilibrium fraction, whereas observations indicate contributions of waters influenced by non-equilibrium processes. This information is quantified using d_{diff} (Figure 2). Positive values of $\delta^{18}O_{diff}$ tended to be associated with negative values of d_{diff} (Figure S8). The shape of the relationship between the two quantities is non-linear, with a stronger relationship between $\delta^{18}O_{diff}$ and d_{diff} among data from arid reaches compared to humid reaches.

The relationship between $\delta^{18}O_{diff}$ and d_{diff}, as well as our regression (Table 2) and surface water line analyses (Table 1) indicate that the modeling approach for estimating long term isotope ratios of rivers produce results that are similar to, but on average, lower and exhibit less variability than observations. The strongest signal in our data is that of evaporation, evidenced by combinations of positive $\delta^{18}O_{diff}$ and negative d_{diff} in arid regions. We also observe evidence of non-equilibrium condensation processes in reaches characterized by negative $\delta^{18}O_{diff}$ and positive d_{diff}.

We suggest that patterns in $\delta^{18}O_{diff}$ and d_{diff} contain useful model diagnostic information that can be useful for improving the NWM and our understanding of the terrestrial water balance. However, the observational dataset is composed of a non-uniform compilation that contains spatial, seasonal, and interannual modes of variability. Due to the underlying sample collection approaches, the strength of our dataset is evaluating spatial variability, so we focus our analysis on that mode to gain information about missing water sources that may influence the model. We support our findings using the temporal evolution of observation-model differences through the growing season. Based on an analysis of the interannual variability (Text S6) we suggest that the spatial and temporal structure of our data are sufficiently robust and evenly distributed with respect to interannual variability to support the analysis. Additional sources of variability are discussed in Text S7.
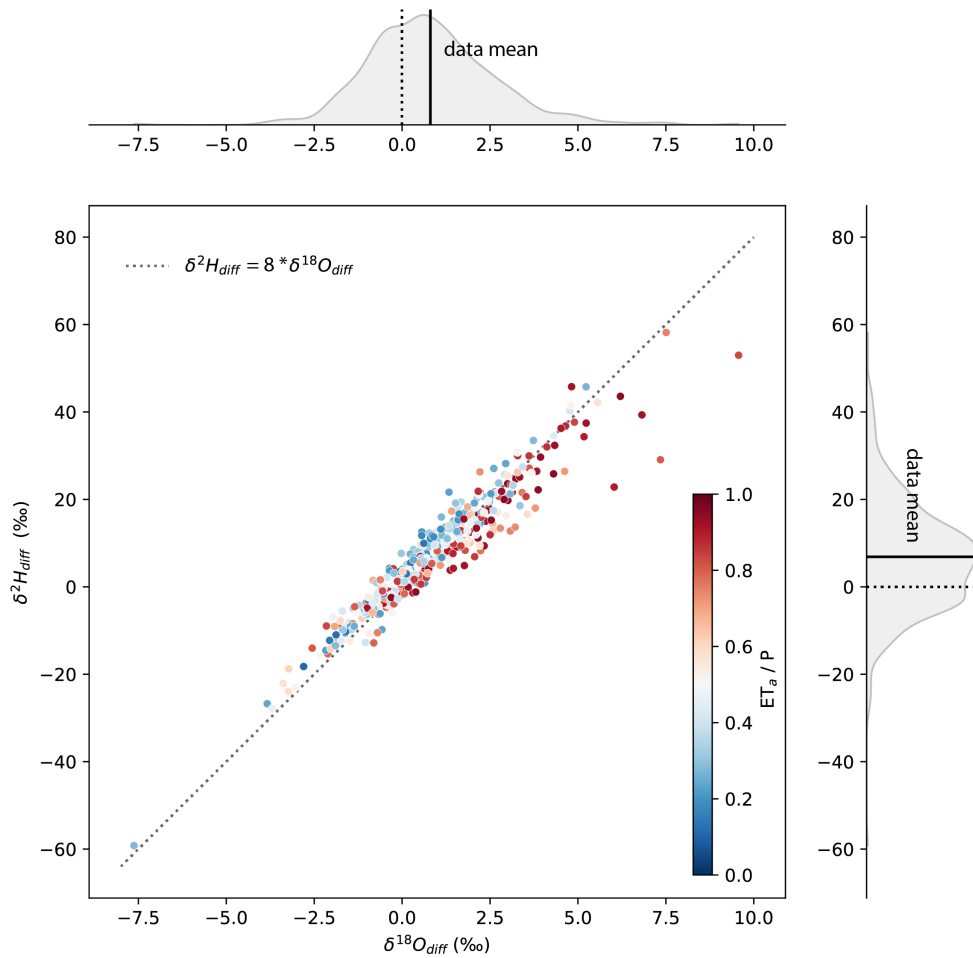
Figure 4. The relationship of observation - isotope mass balance estimation differences for $\delta^{18}O$ and δ^2H. Interpretations of the scatterplot follow the framework indicated in Figure 2. The catchment mean value is plotted, and only sites with at least two observations are shown (n=448). The equilibrium line with slope 8 is plotted for context (dotted line), and data are colored by their site's the ratio of actual evaporation to precipitation. Data distributions are shown for both $\delta^{18}O_{diff}$ and δ^2H_{diff} in the margins, along with the mean differences indicated as a solid line. No difference (0) is marked with a dotted line for reference.

3.3 Spatial distribution of observation - model differences

If the NWM fully constrained all relevant water sources, we expect to observe similar values of $\delta^{18}O_{diff}$ and d_{diff} throughout each basin, irrespective of the location of the observation in the basin. This is because the majority of water discharged to streams in these basins comes from upper elevation water source areas, and based on the assumptions of the NWM framework, little addition or modification of river waters is expected downstream of headwater catchments. Thus, we expect the observation-model differences calculated in headwater areas would propagate to lower elevation areas in the absence of additions from unconstrained water sources and/or river water modifications from unconstrained processes.

Instead, we observed spatial variability (Figures 5 and S9), where smaller magnitude $\delta^{18}O_{diff}$ values occurred in the highest elevation, lowest stream order, and least arid reaches, and larger magnitude, often positive $\delta^{18}O_{diff}$, values occurred in lower elevation, arid or intermittent flow reaches (Figure S10). d_{diff} tended to exhibit higher values in higher elevation, lower stream order reaches, and lower values in lower elevation, more arid, higher stream order reaches (Figure 6). We observed a greater range in the absolute magnitudes of $\delta^{18}O_{diff}$ and d_{diff} in higher order, lower elevation reaches (Figures 6 and S10). Notably, the pattern was similar across basins, suggesting the importance of within-basin processes in determining $\delta^{18}O_{diff}$ an d_{diff}, as opposed to absolute relationships of $\delta^{18}O_{diff}$ and d_{diff} to elevation, stream order, or climate classification.

The spatial pattern in d_{diff} (Figure 5) was similar to the pattern observed for the KGE and other metric evaluations of the NWM (Towler et al., 2023). Areas with negative d_{diff} tended to correspond to areas with poor NWM performance (Towler et al., 2023). However, the isotopic evaluation of NWM and the Towler et al. (2023) datasets could not be directly compared due to there being only a small number of reaches with both isotope observations and daily discharge measurements.

The spatial structure of our results was statistically well explained by the the ratio of actual evaporation to precipitation ($\frac{ET_a}{P}$) in a linear mixed effects model with basin as the grouping variable (Table 3). Variability among basins explained 16.2% of the variance in d_{diff}, while the fixed effect of aridity explained 13.9% of the variability in the dataset. The regression slope associated with the fixed effects of aridity was negative (-7.87$\pm$ 0.78) and significant (p<0.01), indicating that sites with higher aridity indices tended to exhibit more negative d_{diff}. This regression was stronger than a linear mixed effects model with elevation predicting d_{diff}, where the fixed effects of elevation explained 4.7% of the variability in d_{diff}.

Analysis of the spatial variability in our results suggest that 1) higher elevation, lower stream order, perennial, warm temperate or seasonally snowy reaches had small $\delta^{18}O_{diff}$ and positive d_{diff} values and 2) lower elevation, higher stream order, arid and sometimes intermittant stream reaches had larger and more positive $\delta^{18}O_{diff}$ values and more negative d_{diff} values. The first point suggests errors associated with the challenges of providing input values at appropriate temporal resolutions, including representing direct snowmelt contributions o streamflow (Sprenger et al., 2024), whereas the second point suggests the model is missing critical evapoconcentrated water sources in more arid, lower elevation areas of each basin.
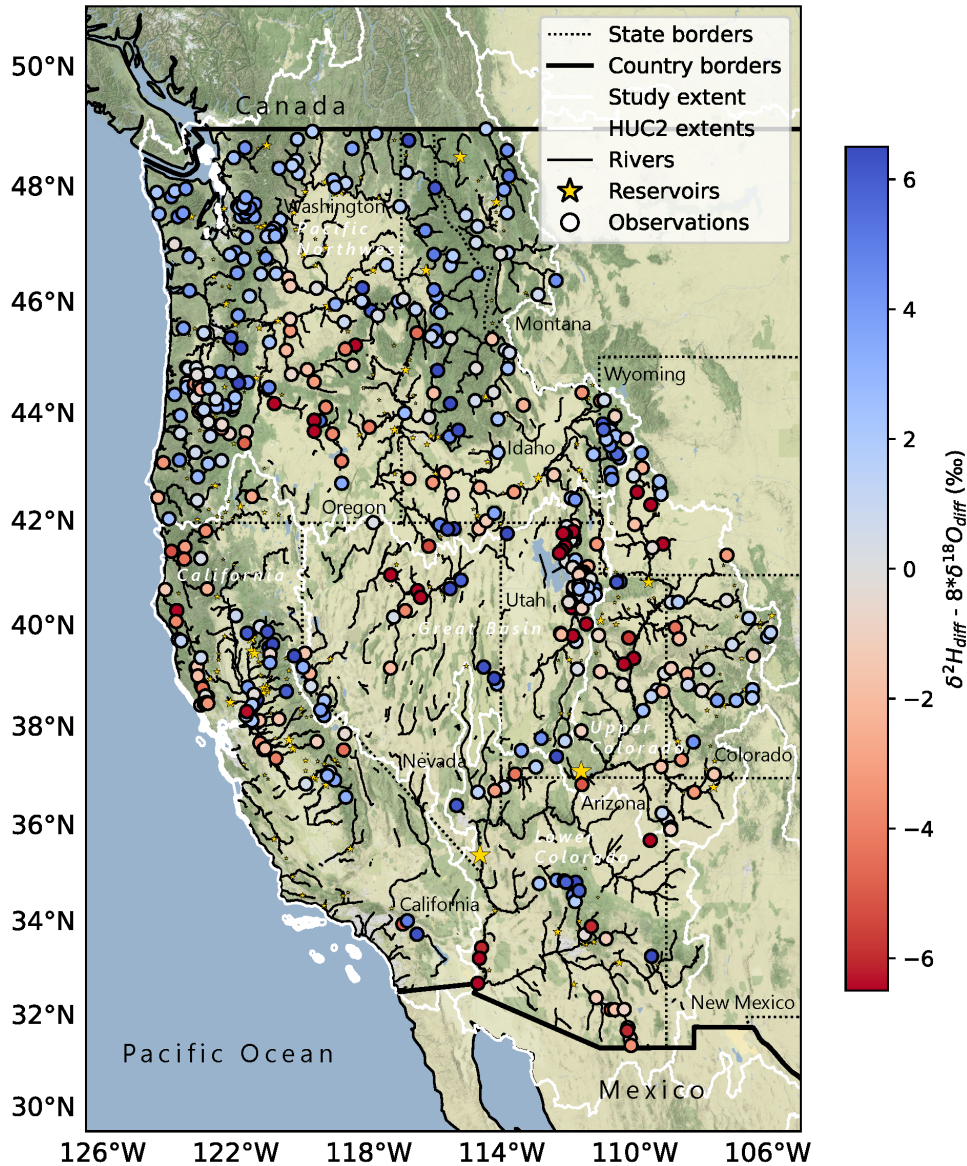
Figure 5. The spatial distribution of mean catchment d_{diff} ($\delta^2 H_{diff} - 8 * \delta^{18}O_{diff}$) in reaches with more than one observation (n=448). Reservoirs are marked by yellow stars, with the star size proportional to the reservoir capacity. Redder symbols correspond to waters with stronger evaporation signals than expected based on the model estimate. Map data is from ©OpenStreetMap contributors 2023, distributed under the Open Data Commons Open Database License (ODbL) v1.0, accessed through Stamen OpenSource Tools (https://stamen.com/open-source/). HUC2 basins come from WBD (U.S. Geological Survey, National Geospatial Technical Operations Center, 2023) and rivers are modified from the NHDPlus streamline network (U.S. Geological Survey, 2019).
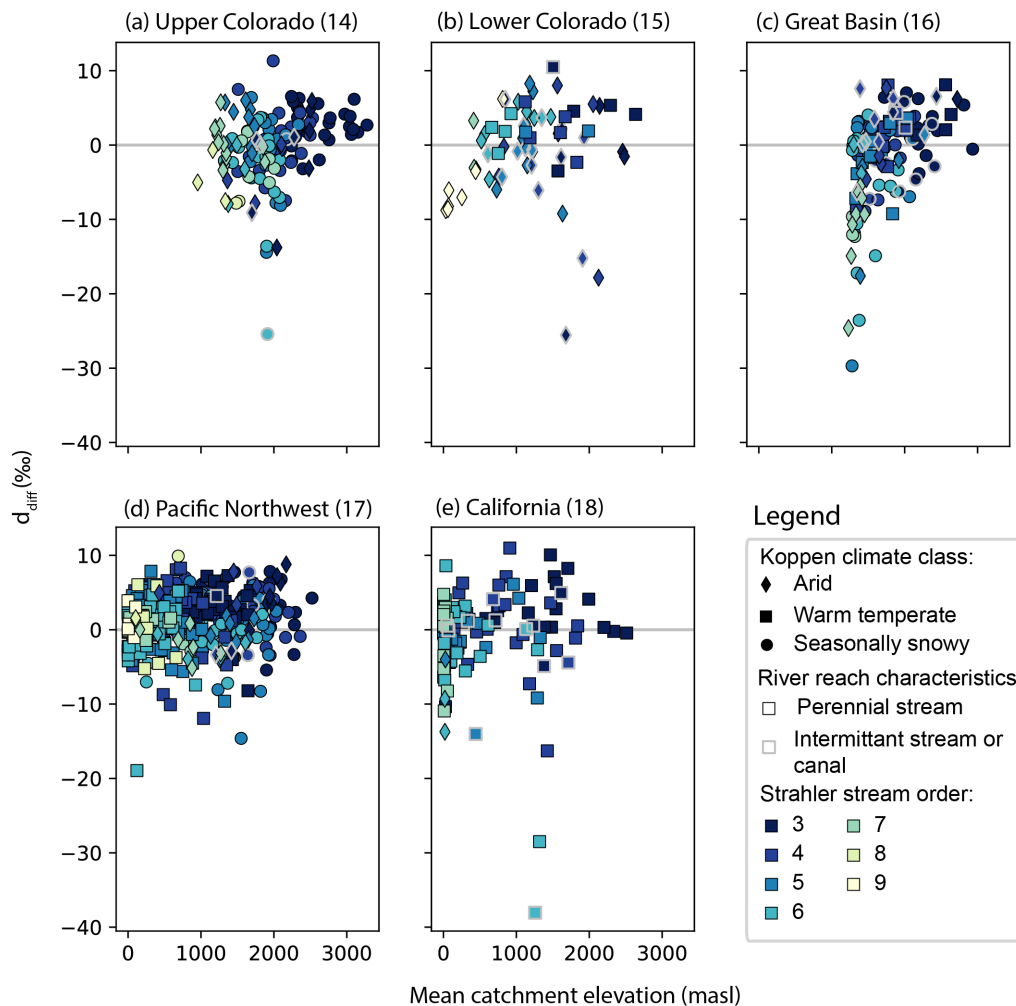
Figure 6. Relationship of elevation, Strahler stream order, and Köppen climate classification (Rubel and Kottek, 2010), and stream persistence to d_{diff} in each basin. We observe higher d_{diff} in perennial, lower order streams at middle and higher elevations in each basin. Lower d_{diff} is associated with higher order streams at lower elevations in each basin. This effect was greater in catchments classified as arid or seasonally snowy compared to those classified as warm temperate. This pattern was generally true in each basin, irrespective of the absolute elevation or stream order, suggesting the importance of accumulated effects within a basin on d_{diff}.

3.3.1 Observation-model differences in headwater reaches reflect groundwater isotope ratio estimates

485 We observe $\delta^{18}O_{diff}$ and d_{diff} values that are statistically different from 0 in higher elevation, low stream order, low aridity, temperate or seasonally snowy reaches in our dataset (Figures 6, S10). These differences tend to be smaller than than the full dataset mean $\delta^{18}O_{diff}$ and d_{diff}. At most of these reaches we also observe positive d_{diff} values (Figures 5, 6).

The presence of both negative and positive values of $\delta^{18}O_{diff}$ likely reflect interannual variability in the isotope ratios of actual groundwater and snowmelt discharged to rivers in high elevation headwater areas. Although groundwater's contribution

490 to streams is conceptualized in this study to be constant in magnitude and isotope ratio, the isotope ratios of both groundwater and snowmelt fluxes vary spatially and interannually. The groundwater flux magnitudes vary interannually based on variations in snowpack magnitudes, antecedent hydrologic conditions (Brooks et al., 2021; Wolf et al., 2023), and hydrogeologic (Gentile et al., 2023) controls including hydrologic residence times. Snowpack isotope ratios vary in response to climate patterns and local conditions (Anderson et al., 2016) and the imprint of snowmelt on river isotope ratios depends on melt timing and

495 contributing elevations (Sprenger et al., 2024). The observed variability of $\delta^{18}O_{diff}$ does not exhibit a uniform tendency towards positive or negative values. This suggests the mean groundwater isotope ratios used in this study are reasonably representative of the long term mean estimates of the isotope ratios of water contributed at high elevation water source areas by groundwater and snowmelt fluxes, though improvements may be made by using a time-varying approach, where estimates of groundwater and snowmelt isotope ratios vary with month and year. However, the systematic positive d_{diff} result cannot be

500 explained by the timescale of the isotope input.

Higher d streamflow relative to weighted mean precipitation values have been documented in other studies (Nickolas et al., 2017). This may be because higher d is associated with lower precipitation $\delta^{18}O$ that falls during the cold season in mid-latitude regions, particularly in areas near open water (Putman et al., 2019; Corcoran et al., 2019; Aemisegger and Sjolte, 2018). Secondarily, high d in rivers relative to precipitation or groundwater may be attributed to fractionation occuring during melt.

505 The snow melt process has been demonstrated to begin with preferential melt of water molecules bearing lighter isotopologues, and to exhibit higher d earlier in the melt season (Ala-aho et al., 2017; Beria et al., 2018; Carroll et al., 2022). Further, a recent study suggested this signal may be used to identify the elevation of snowmelt contributing to streamflow during the melt season (Sprenger et al., 2024). The higher d of the snow and initial meltwater may be passed along to the rivers via direct surface runoff to streams or through shallow groundwater recharge and rapid discharge to streams (see the relatively higher

510 upper bound on d values for forested land use types in Figure 7).
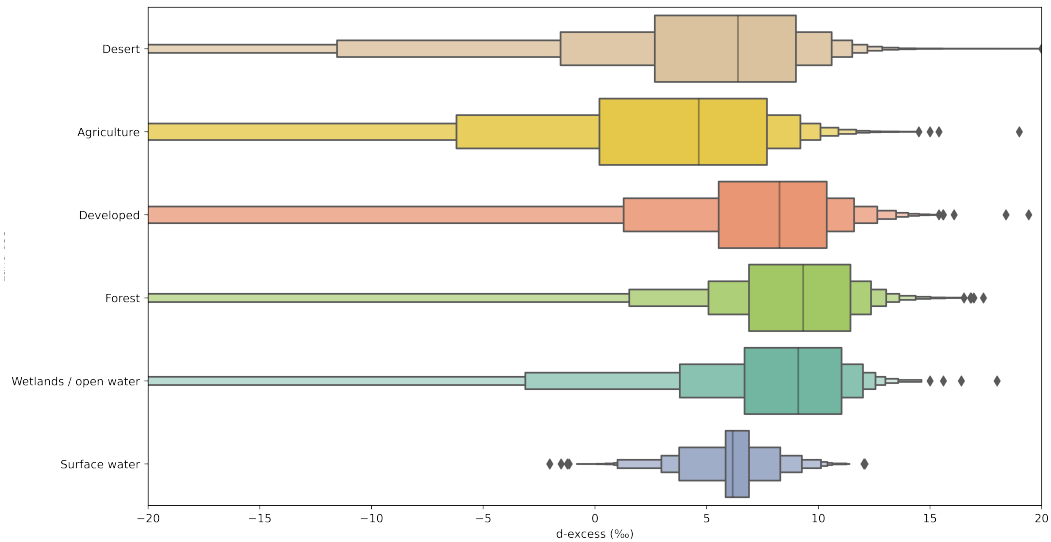
Figure 7. Distributions of groundwater d grouped by the dominant land type from NLCD (Dewitz and U.S. Geological Survey, 2021) in the HUC12 (U.S. Geological Survey, National Geospatial Technical Operations Center, 2023) of the observation. The data are displayed as letter-plots (Heike Hofmann and Kafadar, 2017), where the central line is the data median, the innermost box contains 50% of the data, the remaining boxes each contain 50% of the remaining data, and thus a diminishing proportion of the total data (i.e., 25%, 12.5%, 6.25%, etc). The black diamonds represent outliers. The plot contain between 85 and 95% of the data available for each land type and thus reasonably represents the distribution of d associated with groundwater from each land use type, even though samples with very low d are not shown. The desert land class includes barren land (often playas or dried lakebeds), shrub/scrub, grasslands/herbaceous. The agricultural land class includes pasture/hay and cultivated crops. The developed land class includes developed land of any intensity. Forest includes evergreen, deciduous and mixed forest. The wetlands/open water land class category any type of wetland as well as open water. The distribution of our 4303 river samples is also shown for context.

3.3.2 Isotopic signals of evaporation at low elevations suggests contributions of irrigation return flows to streamflow

Greater spatial and temporal variability in both $\delta^{18}O_{diff}$ and d_{diff} in lower elevation, higher stream order, arid reaches suggests the importance of various spatially and temporally heterogeneous processes and water sources that may alter streamflow isotope ratios relative to upstream values. Positive values of $\delta^{18}O_{diff}$ and negative values of d_{diff} in more arid regions of each basin suggests that evaporated waters compose a non-trivial fraction of streamflow in these areas (Figures 5, 6, S9 and S10), especially in the later part of the growing season (Figure 9) when streams depend more heavily on groundwater fluxes. We observed isotopic evidence of contributions of evaporated waters to rivers in all basins (Figure 6), though it was most apparent in Lower Colorado River Basin, lower elevation regions of the Upper Colorado River Basin, California's Central Valley, near Great Salt Lake in the Great Basin and throughout the Snake River Plain (Figures 5 and S9).

The isotope ratios and d we observe in low elevation, high stream order arid reaches are similar to those we would expect to observe in highly evaporative contexts, like within lakes (Bowen et al., 2018), intermittent flow rivers, or downstream of wetlands. Yet the majority of rivers in our study are perennial, and most are not characterized by substantial wetlands. The evapoconcentration in our dataset is unlikely to arise from river or reservoir evaporation because both evaporation of reservoirs and evaporation to inflow ratios in the region tend to be low, especially for deep man-made reservoirs (Brooks et al., 2014; Friedrich et al., 2018). Instead, isotopic evidence of evapoconcentration occurs in waterways likely to be affected by anthropogenic hydrologic alteration (Fergus et al., 2021) and characterized by larger fractions of 'young water' (Jasechko et al., 2014; Burt et al., 2023; Xia et al., 2023).

We tested the hypothesis that the spatial pattern of isotopically-inferred evaporation could arise from contributions of irrigation return flows to streams and reservoir releases. Within each basin, on average, d_{diff} was most negative, indicating isotopic evidence of evaporation, at sites with the highest proportion of total inflows attributed to agricultural return flows and highest at sites with no apparent contributions of agricultural return flows (Figure 8). Reservoir influence was associated with low d_{diff} more often where dams are used for water management and water supply (e.g., Upper Colorado, Lower Colorado, Great Basin, and California) and were associated with high d_{diff} in the Pacific Northwest, where dams are more often used for hydropower. Intermittent streams and canals in arid regions were sometimes associated with low d_{diff} as well, even when no water was contributed by agricultural irrigation.

We demonstrated the relationships of agricultural and reservoir influence on d_{diff} statistically in a linear mixed effects model (Table 3). The fraction of streamflow estimated to come from agricultural irrigation return flows and a categorical variable delineating reservoir influence together explained 8.0% of the variance in d_{diff}, with the whole model (including random group effects) explaining 14.3% of the variance in the dataset. Both explanatory variables were significant ($p<0.01$), and, as expected, exhibited negative slopes indicating that greater agriculture and reservoir influences tended to produce lower d_{diff} values, indicative of evaporative effects. When we included the ratio of actual evaporation to precipitation with these explanatory variables, all three are significant ($p<0.01$) and explain 15.2% of the variance through fixed effects, and 23.0% of the variance overall (fixed and random effects). Among the linear mixed effects models tested, it exhibited the highest log
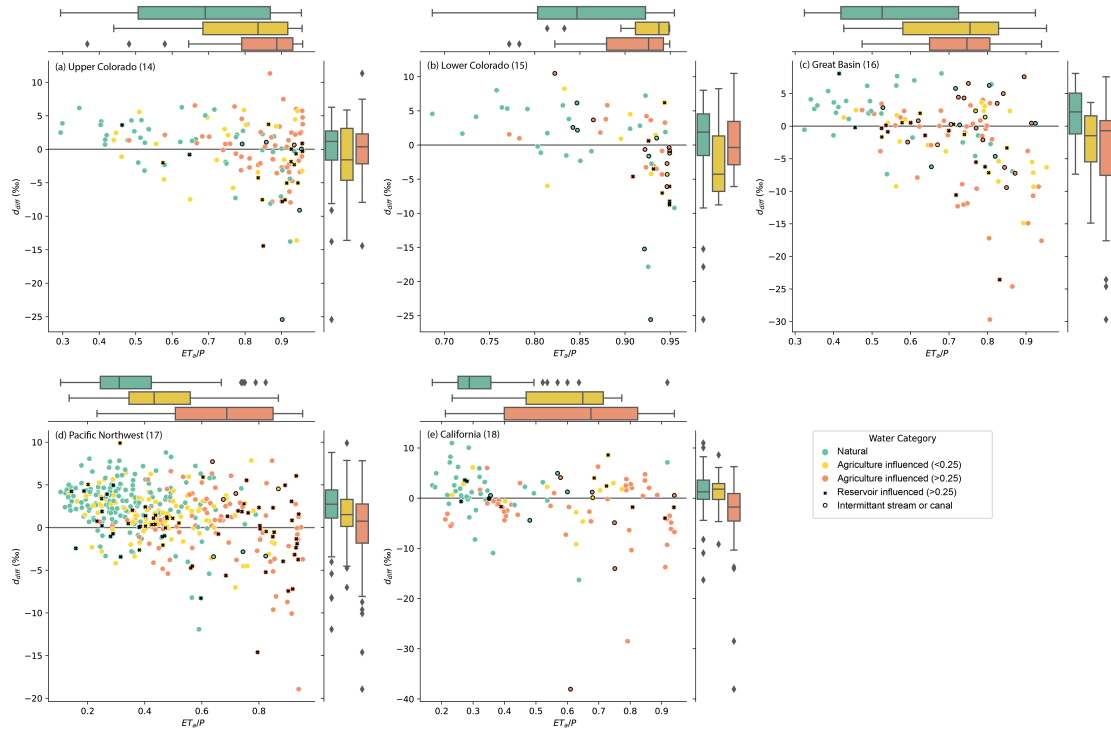
Figure 8. Relationship of aridity to d_{diff}, by water use categories and basins. Natural waters are not estimated to be influenced by agricultural irrigation. Fractions of agricultural irrigation contributing to streamflow are estimated using water use data and land cover data and do not account for losses to evapotranspiration. We identified reaches affected by large reservoirs and reaches categorized as intermittent or as canals or ditches with additional symbology.

likelihood value, explained the greatest amount of variance using fixed effects, and reduced the amount of variance attributed
545 to random within-basin effects.

While this statistical model performance is not substantially better at explaining variance in d_{diff} than the model that uses aridity alone, the findings do suggest that both agricultural activity and reservoirs influence the isotope ratios of streamflows across the Western US. The low variance explained by these models is expected, due to the difficulty estimating true long term mean agricultural return flux with the spatial and temporal resolution of the available data, the confounding influences of
550 season and year on the response variable, the potential for isotopically heterogeneous reservoir effects, the covariance of both irrigation return flows and the presence of reservoirs with aridity and elevation, and the spatially variable effect of irrigation on streamflows (Ketchum et al., 2023). The statistical linkage between irrigation water use and the isotopic response would likely be improved by taking a time-variable approach to estimating river isotope ratios, and the contribution of irrigation water in the river, which may be doable with improvement to both precipitation isotope datasets and higher spatial and temporal resolution
555 irrigation water use datasets (e.g., Haynes et al.).

Statistical model	β ($\pm$ s.e.)	I ($\pm$ s.e.)	HUC2 (group)	Cond. R^2	Fixed R^2	Log likeli-hood
$d_{diff} \sim Elev + I$	$Elev$: 0.001 (0.00)*	-1.93 (1.01)	4.33	20.9%	4.4%	-2254
$d_{diff} \sim \frac{ET}{P} + I$	$\frac{ET}{P}$: -7.85 (0.77)*	4.86 (1.08)*	4.37	30.2%	13.9%	-2209
$d_{diff} \sim F_{irr} + Res + I$	F_{irr}: -3.49 (0.48)* Res: -1.75 (0.45)*	0.95 (0.59)	1.43	14.3%	8.0%	-2224
$d_{diff} \sim \frac{ET}{P} + F_{irr} + I$	$\frac{ET}{P}$: -6.50 (0.88)* F_{irr}: -1.60 (0.54)*	4.39 (0.83)*	1.941	22.8%	14.8%	-2204
$d_{diff} \sim \frac{ET}{P} + F_{irr} + Res + I$	$\frac{ET}{P}$: -6.08 (0.88)* F_{irr}: -1.67 (0.54)* Res: -1.22 (0.44)*	4.32 (0.82)*	1.861	23.0%	15.2%	-2200

Table 3. Results of linear mixed effects models with 764 observations and 5 groups. The minimum and maximum group sizes were 48 and 387, respectively. The models do not include any samples from reaches characterized as an intermittent stream or canal or where NWM indicates that the maximum streamflow is 0 m^3 s^{-1}. Random effects apply only to the intercepts. An asterisk indicates that a regression coefficient is statistically significant at p<0.01. Conditional R^2, which gives the total model variance explained, are reported alongside the fixed R^2, which gives the variance explained by fixed effects (i.e., explanatory variables) and the log-likelihood, which can be used to evaluate the relative performance of different models.

3.4 Further evidence supporting irrigation contributions to streamflow

We have statistically quantified isotopic evidence for irrigation contributions to streamflow. However, the statistical model performance is not substantially better at explaining variance in d_{diff} than the model that uses aridity alone. To further investigate our findings, we include analyses of additional lines of evidence. We evaluate signals embedded in seasonal patterns in our dataset, as well other studies, spatial variability in groundwater isotope ratios, and evaluation of the NWM with a well level relative to river level dataset.

3.4.1 Seasonal patterns in observation-model differences

There are systematic patterns in $\delta^{18}O_{diff}$ and d_{diff} when examined across the growing season that support our spatial assessment of the contributions of irrigation to streamflow. For example, $\delta^{18}O_{diff}$ tends to be greater during the latter months of the growing season relative to the mean $\delta^{18}O_{diff}$ value for the month of June for that site and year (Figure 9a) in most basins and months. The pattern is especially evident in the Great Basin and California. Likewise, d_{diff} is lower in July, August, September relative to June (Figure 9b), in the Great Basin and California. The contrast between basins with both increased $\delta^{18}O_{diff}$ and decreased d_{diff} (Great Basin and California) and those with only increased $\delta^{18}O_{diff}$ and little change in d_{diff} (Upper and Lower Colorado and Pacific Northwest) suggests that two different mechanisms may drive isotopic change during the growing season.

In California and the Great Basin, which are characterized by $\delta^{18}O_{diff}$ increases and d_{diff} decreases over the growing season relative to June, we suggest increased contributions of evaporated waters to rivers later in the growing season. In California, this may reflect the water use and irrigation return flows contributing to streamflow in the Central Valley.

In the Upper and Lower Colorado and Pacific Northwest, where we observe small $\delta^{18}O_{diff}$ increases and little d_{diff} change relative to June, we suggest sustained dependence on groundwater discharge from high elevations to streamflow during the growing season (Miller et al., 2016; McGill et al., 2021; Windler et al., 2021). In downstream sections of the Upper Colorado and the Lower Colorado, where rivers are characterized by discharges from large reservoirs, the seasonal invariance may reflect that the primary 'water source' regions for these reaches are reservoirs, which retain snowmelt from early in the season and discharge it later in the season.
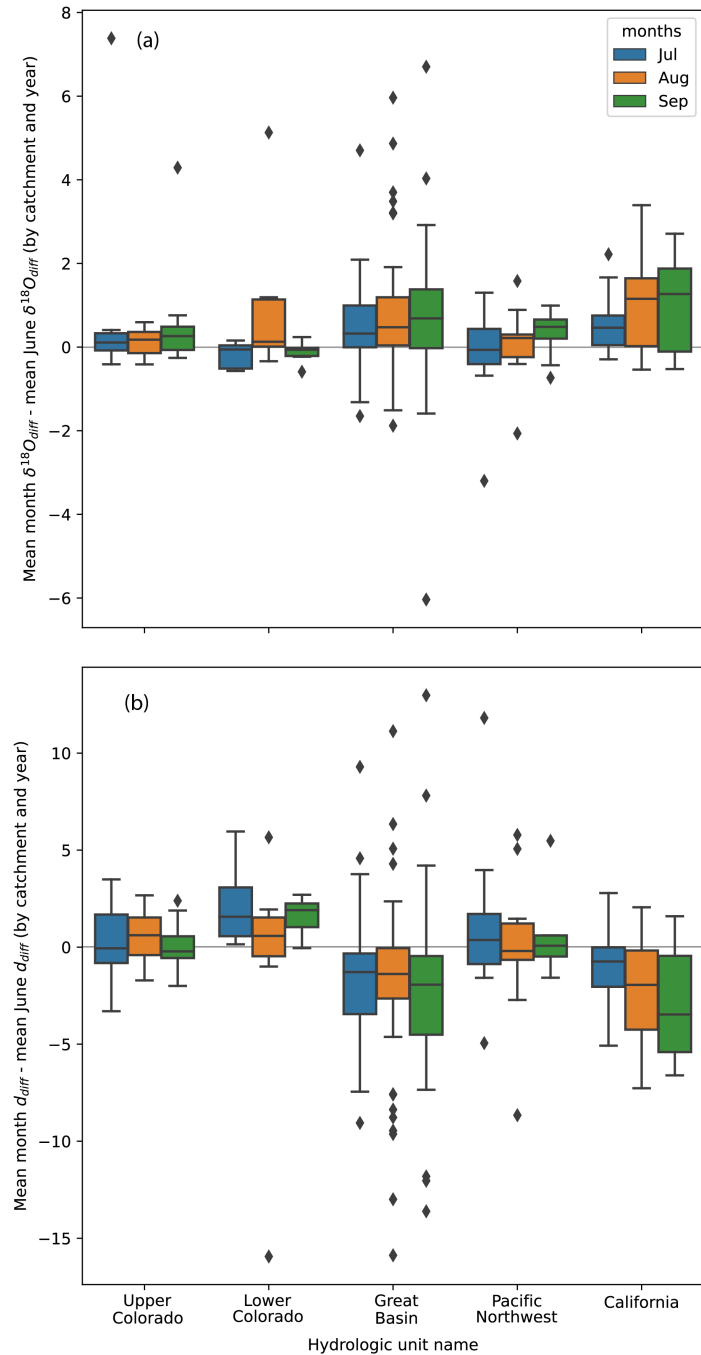
Figure 9. Evaluation of seasonal variability in observation-model comparisons. Data include all reaches and years with collections in the month of June as well as 2 of the 3 other months of the summer season. (a) The distribution (represented by boxplots) of month-specific differences from June $\delta^{18}O_{diff}$ by basin. (b) The distribution (represented by boxplots) of month-specific differences from June d_{diff}. The boxplots show the median, 25th and 75th percentiles as the box, whiskers extend to points that lie within 1.5 IQRs of the lower and upper quartile, and observations that fall outside this range are displayed as diamonds.

3.4.2 Literature and other datasets

Numerous prior studies have investigated the influence of irrigation on streamflow. Estimates suggest that, depending on the irrigation type, as much as 50% of applied water may recharge groundwater and/or arrive at surface waters through shallow groundwater infiltration and subsequent discharge to streams (Grafton et al., 2018). Likewise, irrigation has been demonstrated to increase streamflows during low flow periods (Fillo et al., 2021; Essaid and Caldwell, 2017), if the applied water comes from surface water diversions.

Local contributions of groundwater to streams from irrigation-based recharge are supported by the d values of groundwater in agricultural regions. Groundwater from regions influenced by agricultural irrigation exhibited lower mean d relative to deserts, including dried terminal lakes and playas, developed areas which may include turf grass irrigation, forested regions, wetlands or open waters and surface waters (Figure 7). Based on the isotope ratios of groundwater in irrigated areas and prior isotopic inference (Windler et al., 2021), we hypothesize that inclusion of irrigation-recharged groundwater discharge as a source of water to streams in NWM would decrease the difference between modeled and observed isotope ratios in our dataset.

The isotopic inference that irrigation return flows are an important missing process in the NWM is supported by an independent statistical comparison of the NWM groundwater discharge with the Jasechko et al. (2021) dataset and the agricultural water use data. The Jasechko et al. (2021) data is the fraction of well water levels that lie below the proximal river water level in a catchment and provides some estimate of hydraulic head and direction of groundwater-surfacewater exchange. When the fraction is high, the river (under correct permeability conditions) would be expected to lose water to groundwater, whereas when the fraction is low the river would be expected to gain water from groundwater discharge.

We hypothesize that if NWM accurately represents groundwater discharge to streams, the Jasechko et al. (2021) well water level comparison to stream water level dataset should be able to predict the summer mean NWM groundwater discharge flux with a large proportion of variance explained. However, the Jasechko et al. (2021) data weakly (R^2 = 0.028, p<0.01) predict the NWM groundwater discharge rates in a simple linear regression. The regression relationship between the variables is negative, as expected, where river reaches with a greater proportion of their well water levels above proximal river water levels correspond to reaches with greater groundwater discharge fluxes (Figure S11). Though the regression is significant, it has almost no predictive capacity, contrary to expectations.

The weakness of the statistical relationship between the Jasechko et al. (2021) dataset and the NWM groundwater discharge flux may be related to shallow aquifers, which are not considered by NWM, and/or agricultural irrigation, as well as the water source (surface or ground water) used for that irrigation (Figure S12). We did not assess the potential for NWM groundwater discharge to reflect the presence of shallow aquifers. However, we observe that the influence of irrigation on groundwater levels is non-stationary, depending on both the groundwater discharge magnitude as well as the source of irrigation water. For this reason the relationship is difficult to assess statistically. In river reaches where NWM indicates little groundwater discharge (0th to 20th percentile qBucket), irrigation sourced from surface water is associated with a smaller fraction of well water levels below river level (smaller y value in Figure S12) than those without irrigation. Conversely, in river reaches with substantial groundwater discharge (80th to 100th percentile qBucket), agricultural irrigation with water from either surface or

groundwater tends to be associated with a larger fraction of well water levels below river level (larger y value in figure S12) compared to reaches without any agricultural irrigation. Based on these patterns we suggest that in dry areas, irrigation from surface water appears to contribute to groundwater recharge, whereas in wet areas, irrigation appears to contribute to decreased water table elevations. At all groundwater discharge percentiles, surface water irrigation contributes to higher water tables, whereas irrigation from groundwater contributes to lower water tables.

Some part of this signal is regional. Reaches from more arid basins compose a greater proportion of the lower percentile qBucket reaches, and reaches from humid or seasonally snowy basins compose a greater proportion of the higher percentile qBucket reaches. However, when evaluated by basin, the relationships are similar. The finding is consistent with modeling studies, which showed lower stream discharge when irrigation water came from groundwater, and greater stream discharge when irrigation water came from surface water (Essaid and Caldwell, 2017). Our analysis suggests that agricultural irrigation is likely to influence groundwater levels and groundwater discharge on a landscape scale and produces gaining streams and contributes to streamflow in otherwise arid, losing reaches of rivers.

3.5 Implications of including irrigation return flows into NWM calculations

Our evaluation of the NWM-driven isotope mass balance calculations suggest that the NWM accuracy would be improved by including agricultural return flows in the water sources sustaining streamflow in the NWM. In effect, agricultural return flows are simply groundwater fluxes to streams that occur at lower elevations than the majority of the groundwater discharge sustaining streams. Based on magnitudes of d_{diff}, these lower elevation groundwater fluxes can sometimes be large. Because the NWM is calibrated to actual streamflows which contain these return flows, these fluxes are currently being misallocated in the model. Inaccuracies in any model terms or fluxes influence the model's capacity to project accurate streamflows, particularly under non-stationary hydrologic conditions. Accurate model water source inclusion, particularly at low elevations where water use and availability is most critical, thus has implications for the model's utility to stakeholders, including water managers and users.

Under current conditions, agricultural return flows may be critical for sustaining streamflow late in the growing season (August or September) or during drought periods. Sustained streamflow in certain reaches is critical for 1) water access for surface water diversions and 2) water availability for species' use. For example, protected fish species survival requires that waterways meet thresholds of water quality, temperature, and depth for survival (Dibble et al., 2020). Water managers make decisions about water allocations and reservoir releases in part to meet these habitat needs (Bruckerhoff et al., 2022). Agricultural return flows have the capacity to help sustain streamflow (Fillo et al., 2021), but with potentially negative effects on water quality, through agriculture-associated salinization (Miller et al., 2017; Thorslund et al., 2021; Miller et al., 2024; Putman et al., 2024), increased concentrations of nitrate (Lin et al., 2021), and other nutrients (Stets et al., 2020), contributions of pesticide and fertilizers, or alterations to water temperature profiles. These contributions of agricultural waters contribute to sustaining flow but threaten water availability. Thus, inclusion of groundwater return flows from irrigation to rivers in the Western US supports improved assessments of water availability both through improved modeling of streamflows and enhanced ability to model water quality.

Explicit inclusion of irrigation return flows will assist the NWM in better projecting streamflows during periods of hydrologic non-stationarity, as are likely to characterize the hydroclimatic elements of climate change. Non-stationary processes include hydrologic changes arising from the ongoing mega-drought of the southwestern US (Williams et al., 2022), associated changes in water use for irrigation (Ketchum et al., 2023), intense precipitation events like monsoons or major storm events that are observed to be increasing in intensity with climate change (Pfahl et al., 2017; Demaria et al., 2019), and projected changes to future snowpack depth and melt timing (Siirila-Woodburn et al., 2021; Hammond et al., 2023). The ongoing aridification of the southwestern US is characterized by increased evapotranspiration (Milly and Dunne, 2020), and changes to groundwater recharge and discharge associated with decreases in snowpack and changes to snowpack melt patterns (Hammond et al., 2023). Understanding the groundwater flux contributions of areas with shallow water tables to streamflow during major precipitation events will help better characterize areas at risk for flooding and inform appropriate water management strategies.

4 Conclusions

The isotope mass balance evaluation of the NWM revealed similarities between the isotope mass balance estimated isotope ratios (modeled) and observed isotope ratios. The mass balance approach represented as much as 75% of the variance in the observations, depending on the water isotopologue evaluated. This suggests that, on average, during the summer, the NWM correctly represents the relative proportions of groundwater and surface runoff fluxes sustaining streamflow, and the gridded isotope datasets are appropriate for the analysis.

The observation-model differences exhibited spatial and seasonal structure, suggesting that the NWM is missing important additional water sources that contribute to streamflow. Specifically, the observation-model differences that plot above the equilibrium line (Figure 2) suggest the importance of direct contributions of snowmelt to streamflow in humid areas. Those that plot below the equilibrium line suggest the importance of groundwater sources characterized by evaporation in arid areas. We tested the hypothesis that agricultural irrigation return flows are the missing evaporated water source in arid regions, and found them to be a significant predictor of observation-model differences. Future work may benefit from taking a time-varying approach to estimation of streamflows and agricultural contributions to streams, as the difference in timescale between the observations and models is a source of uncertainty. Nonetheless, our finding is supported by multiple lines of evidence including the seasonality of observation-model differences, relationship of land use to isotopic signals (d) of evaporation in groundwaters, a comparison of NWM groundwater discharge with an independent assessment of the potential for groundwater discharge and isotopic and modeling study conclusions from the literature.

Our findings suggest that the NWM accuracy would be improved by including agricultural irrigation fluxes into the NWM water sources. Agricultural irrigation recharged groundwater functions as lower elevation baseflow fluxes, and are likely to be critical for sustaining streamflow during drought periods or late in the growing season. Inclusion of this specific source into groundwater fluxes would improve the ability to meet water manager and water user NWM data needs. Specifically, water managers use predictions of reach-specific flows at lower elevations during summer precipitation events and monsoons to assess flood risk, or to inform dam releases (if dam releases are incorporated into the NWM) to assess the volume of water required to

achieve specific management goals like fish species preservation or dam water level maintenance for hydropower production. Likewise, explicit inclusion of irrigation return flows in NWM calculations will assist in accurately predicting and projecting streamflows in heavily managed sections of river in the event of changing irrigation practices, increased evapotranspiration, or water supply reductions and fallowing of agricultural fields, which would change or halt irrigation groundwater fluxes. Finally, our findings have implications for areas at risk for diminished water availability due to issues of quality, arising from the entrainment of fertilizer and pesticides and as well as dissolution and delivery of salts.

Data availability. Data are publicly available (Reddy et al., 2023).

Author contributions. Conceptualization and funding acquisition: ALP and OLM; Data curation: PCL, MCM, MK, JR, and JRB; Methodology, investigation and formal analysis: ALP and PCL; Project administration and supervision: ALP; Visualization: ALP; writing (original draft): ALP; Writing - review: OLM, PCL, MCM, JR, MK and JRB

Competing interests. The authors declare no competing interests

Acknowledgements. The authors acknowledge financial support from the US Geological Survey (USGS) Water Mission area Water Quality Processes Division. We appreciate comments from two USGS peer reviewers, whose comments improved the quality of the manuscript. The views expressed in this article are those of the author(s) and do not necessarily represent the views or the policies of the US Environmental Protection Agency. Any use of trade, firm, or product names is for descriptive purposes only and does not imply endorsement by the US Government..

References

Aemisegger, F. and Sjolte, J.: A Climatology of Strong Large-Scale Ocean Evaporation Events. Part II: Relevance for the Deuterium Excess Signature of the Evaporation Flux, Journal of Climate, 31, 7313 – 7336, https://doi.org/https://doi.org/10.1175/JCLI-D-17-0592.1, 2018.

Ala-aho, P., Tetzlaff, D., McNamara, J. P., Laudon, H., Kormos, P., and Soulsby, C.: Modeling the isotopic evolution of snowpack and snowmelt: Testing a spatially distributed parsimonious approach, Water Resources Research, 53, 5813–5830, https://doi.org/https://doi.org/10.1002/2017WR020650, 2017.

Anderson, L., Berkelhammer, M., and Mast, M. A.: Isotopes in North American Rocky Mountain Snowpack 1993–2014, Quaternary Science Reviews, 131, 262–273, https://doi.org/https://doi.org/10.1016/j.quascirev.2015.03.023, 2016.

Barnhart, T. B., Molotch, N. P., Livneh, B., Harpold, A. A., Knowles, J. F., and Schneider, D.: Snowmelt rate dictates streamflow, Geophysical Research Letters, 43, 8006–8016, https://doi.org/https://doi.org/10.1002/2016GL069690, 2016.

Beria, H., Larsen, J. R., Ceperley, N. C., Michelon, A., Vennemann, T., and Schaefli, B.: Understanding snow hydrological processes through the lens of stable water isotopes, WIREs Water, 5, e1311, https://doi.org/https://doi.org/10.1002/wat2.1311, 2018.

Bowen, G.: The Online Isotopes in Precipitation Calculator, version 2.0, https://wateriso.utah.edu/waterisotopes/pages/information/oipc_info.html, 2006.

Bowen, G.: The Online Isotopes in Precipitation Calculator, version 3.1, http://www.waterisotopes.org, 2022a.

Bowen, G. J.: Spatial analysis of the intra-annual variation of precipitation isotope ratios and its climatological corollaries, Journal of Geophysical Research: Atmospheres, 113, https://doi.org/https://doi.org/10.1029/2007JD009295, 2008.

Bowen, G. J.: Gridded maps of the isotopic composition of meteoric waters, http://www.waterisotopes.org, uSA grids downloaded Nov 2021, 2022b.

Bowen, G. J. and Revenaugh, J.: Interpolating the isotopic composition of modern meteoric precipitation, Water Resources Research, 39, 1299, https://doi.org/10.1029/2003WR002086, 2003.

Bowen, G. J., Wassenaar, L. I., and Hobson, K. A.: Global application of stable hydrogen and oxygen isotopes to wildlife forensics, Oecologia, 143, 337–348, https://doi.org/10.1007/s00442-004-1813-y, 2005.

Bowen, G. J., Putman, A. L., Brooks, J. R., Bowling, D. R., Oerter, E. J., and Good, S. P.: Inferring the source of evaporated waters using stable H and O isotopes, Oecologia, 187, 1025–1039, https://doi.org/10.1007/s00442-018-4192-5, 2018.

Bowen, G. J., Cai, Z., Fiorella, R. P., and Putman, A. L.: Isotopes in the water cycle: Regional-to global-scale patterns and applications, Annual Review of Earth and Planetary Sciences, 47, https://doi.org/10.1146/annurev-earth-053018-060220, 2019.

Bowen, G. J., Guo, J. S., and Allen, S. T.: A 3-D groundwater isoscape of the contiguous USA for forensic and water resource science, PLOS ONE, pp. 1–22, https://doi.org/10.1371/journal.pone.0261651, 2022.

Brooks, J. R., Gibson, J. J., Birks, S. J., Weber, M. H., Rodecap, K. D., and Stoddard, J. L.: Stable isotope estimates of evaporation : inflow and water residence time for lakes across the United States as a tool for national lake water quality assessments, Limnology and Oceanography, 59, 2150–2165, https://doi.org/https://doi.org/10.4319/lo.2014.59.6.2150, 2014.

Brooks, P. D., Gelderloos, A., Wolf, M. A., Jamison, L. R., Strong, C., Solomon, D. K., Bowen, G. J., Burian, S., Tai, X., Arens, S., Briefer, L., Kirkham, T., and Stewart, J.: Groundwater-Mediated Memory of Past Climate Controls Water Yield in Snowmelt-Dominated Catchments, Water Resources Research, 57, e2021WR030 605, https://doi.org/https://doi.org/10.1029/2021WR030605, 2021.

Bruckerhoff, L. A., Wheeler, K., Dibble, K. L., Mihalevich, B. A., Neilson, B. T., Wang, J., Yackulic, C. B., and Schmidt, J. C.: Water Storage Decisions and Consumptive Use May Constrain Ecosystem Management under Severe Sustained Drought, JAWRA Journal of the American Water Resources Association, 58, https://doi.org/https://doi.org/10.1111/1752-1688.13020, 2022.

735 Bureau of Reclamation, Department of the Interior: Interior Department Announces Actions to Protect Colorado River System, Sets 2023 Operating Conditions for Lake Powell and Lake Mead, Bureau of Reclamation News; Multimedia, https://www.usbr.gov/newsroom/#/news-release/4294, accessed Aug 18, 2022, 2022.

Burt, E. I., Coayla Rimachi, D. H., Ccahuana Quispe, A. J., Atwood, A., and West, A. J.: Isotope-derived young water fractions in streamflow across the tropical Andes mountains and Amazon floodplain, Hydrology and Earth System Sciences, 27, 2883–2898,
740 https://doi.org/10.5194/hess-27-2883-2023, 2023.

Carroll, R. W. H., Deems, J., Maxwell, R., Sprenger, M., Brown, W., Newman, A., Beutler, C., Bill, M., Hubbard, S. S., and Williams, K. H.: Variability in observed stable water isotopes in snowpack across a mountainous watershed in Colorado, Hydrological Processes, 36, e14 653, https://doi.org/https://doi.org/10.1002/hyp.14653, 2022.

Condon, L. E. and Maxwell, R. M.: Simulating the sensitivity of evapotranspiration and streamflow to large-scale groundwater depletion,
745 Science Advances, 5, eaav4574, https://doi.org/https://dx.doi.org/10.1126/sciadv.aav4574, 2019.

Cook, P. G. and Solomon, D. K.: Transport of Atmospheric Trace Gases to the Water Table: Implications for Groundwater Dating with Chlorofluorocarbons and Krypton 85, Water Resources Research, 31, 263–270, https://doi.org/https://doi.org/10.1029/94WR02232, 1995.

Corcoran, M. C., Thomas, E. K., and Boutt, D. F.: Event-Based Precipitation Isotopes in the Laurentian Great Lakes Region Reveal Spatiotemporal Patterns in Moisture Recycling, Journal of Geophysical Research: Atmospheres, 124, 5463–5478,
750 https://doi.org/https://doi.org/10.1029/2018JD029545, 2019.

Craig, H.: Isotopic Variations in Meteoric Waters, Science, 133, 1702–1703, http://www.jstor.org/stable/1708089, 1961.

Craig, H. and Gordon, L. I.: Deuterium and oxygen 18 variations in the ocean and marine atmosphere, in: Stable Isotopes in Oceanographic Studies and Paleotemperatures, p. 9, 1965.

Demaria, E. M. C., Hazenberg, P., Scott, R. L., Meles, M. B., Nichols, M., and Goodrich, D.: Intensification of the North Ameri-
755 can Monsoon Rainfall as Observed From a Long-Term High-Density Gauge Network, Geophysical Research Letters, 46, 6839–6847, https://doi.org/https://doi.org/10.1029/2019GL082461, 2019.

Dewitz, J. and U.S. Geological Survey: National Land Cover Database (NLCD) 2019 Products (ver. 2.0, June 2021), https://doi.org/https://doi.org/10.5066/P9KZCM54, 2021.

Dibble, K., Yackulic, C., and Bestgen, K.: Water temperature models, data and code for the Colorado, Green, San Juan, Yampa, and White
760 rivers in the Colorado River basin, https://doi.org/https://doi.org/10.5066/P9HFKV7Q, 2020.

Dieter, C., Maupin, M., Caldwell, R., Harris, M., Ivahnenko, T., Lovelace, J., Barber, N., and Linsey, K.: Estimated use of water in the United States in 2015: U.S. Geological Survey Circular 1441, Tech. rep., U.S. Geological Survey, https://doi.org/https://doi.org/10.3133/cir1441, 2018.

Essaid, H. I. and Caldwell, R. R.: Evaluating the impact of irrigation on surface water – groundwater interac-
765 tion and stream temperature in an agricultural watershed, Science of The Total Environment, 599-600, 581–596, https://doi.org/https://doi.org/10.1016/j.scitotenv.2017.04.205, 2017.

Evaristo, J., Jasechko, S., and McDonnell, J.: lobal separation of plant transpiration from groundwater and streamflow, Nature, 525, 91–94, https://doi.org/https://doi.org/10.1038/nature14983, 2015.

Feng, X., Faiia, A. M., and Posmentier, E. S.: Seasonality of isotopes in precipitation: A global perspective, Journal of Geophysical Research: Atmospheres, 114, https://doi.org/https://doi.org/10.1029/2008JD011279, 2009.

Fergus, C. E., Brooks, J. R., Kaufmann, P. R., Herlihy, A. T., Pollard, A. I., Weber, M. H., and Paulsen, S. G.: Lake Water Levels and Associated Hydrologic Characteristics in the Conterminous U.S., Journal of the American Water Resources Association, 56, 450–471, https://doi.org/https://doi.org/10.1111/1752-1688.12817, 2020.

Fergus, C. E., Brooks, J. R., Kaufmann, P. R., Pollard, A. I., Herlihy, A. T., Paulsen, S. G., and Weber, M. H.: National framework for ranking lakes by potential for anthropogenic hydro-alteration, Ecological Indicators, 122, 107 241, https://doi.org/https://doi.org/10.1016/j.ecolind.2020.107241, 2021.

Fergus, C. E., Brooks, J. R., Kaufmann, P. R., Pollard, A. I., Mitchell, R., Geldhof, G. J., Hill, R. A., Paulsen, S. G., Ringold, P., and Weber, M.: Natural and anthropogenic controls on lake water-level decline and evaporation-to-inflow ratio in the conterminous United States, Limnology and Oceanography, 67, 1484–1501, https://doi.org/https://doi.org/10.1002/lno.12097, 2022.

Fillo, N. K., Bhaskar, A. S., and Jefferson, A. J.: Lawn Irrigation Contributions to Semi-Arid Urban Baseflow Based on Water-Stable Isotopes, Water Resources Research, 57, e2020WR028 777, https://doi.org/https://doi.org/10.1029/2020WR028777, 2021.

Friedrich, K., Grossman, R. L., Huntington, J., Blanken, P. D., Lenters, J., Holman, K. D., Gochis, D., Livneh, B., Prairie, J., Skeie, E., Healey, N. C., Dahm, K., Pearson, C., Finnessey, T., Hook, S. J., and Kowalski, T.: Reservoir Evaporation in the Western United States: Current Science, Challenges, and Future Needs, Bulletin of the American Meteorological Society, 99, 167 – 187, https://doi.org/https://doi.org/10.1175/BAMS-D-15-00224.1, 2018.

Gabor, R. S., Hall, S. J., Eiriksson, D. P., Jameel, Y., Millington, M., Stout, T., Barnes, M. L., Gelderloos, A., Tennant, H., Bowen, G. J., Neilson, B. T., and Brooks, P. D.: Persistent Urban Influence on Surface Water Quality via Impacted Groundwater, Environmental Science & Technology, 51, 9477–9487, https://doi.org/10.1021/acs.est.7b00271, 2017.

Gentile, A., Canone, D., Ceperley, N., Gisolo, D., Previati, M., Zuecco, G., Schaefli, B., and Ferraris, S.: Towards a conceptualization of the hydrological processes behind changes of young water fraction with elevation: a focus on mountainous alpine catchments, Hydrology and Earth System Sciences, 27, 2301–2323, https://doi.org/10.5194/hess-27-2301-2023, 2023.

Gochis, D., Barlage, M., Dugger, A., Karsten, L., McAllister, M., McCreight, J., Mills, J., RafieeiNasab, A., Read, L., Sampson, K., Yates, D., and Yu, W.: The WRF-Hydro Modeling System Technical Description (Version 5.0), Tech. rep., National Center for Atmospheric Research, https://doi.org/https://doi.org/10.5065/D6J38RBJ, nCAR Technical Note, 2018.

Gochis, D., Barlage, M., Cabell, R., Dugger, A., Fanfarillo, A., FitzGerald, K., McAllister, M., McCreight, J., RafieeiNasab, A., Read, L., Frazier, N., Johnson, D., Mattern, J. D., Karsten, L., Mills, T. J., and Fersch, B.: WRF-Hydro v5.1.1, https://doi.org/https://doi.org/10.5281/zenodo.3625238, dataset, 2020a.

Gochis, D. J., Barlage, M., Cabell, R., Casali, M., Dugger, A., FitzGerald, K., McAllister, M., McCreight, J., RafieeiNasab, A., Read, L., Sampson, K., Yates, D., and Zhang, Y.: The WRF-Hydro modeling system technical description, (Version 5.1.1), Tech. rep., UCAR, https://ral.ucar.edu/sites/default/files/public/projects/wrf-hydro/technical-description-user-guide/wrf-hydrov5.2technicaldescription.pdf, nCAR Technical Note, 2020b.

Grafton, R. Q., Williams, J., Perry, C. J., Molle, F., Ringler, C., Steduto, P., Udall, B., Wheeler, S. A., Wang, Y., Garrick, D., and Allen, R. G.: The paradox of irrigation efficiency, Science, 361, 748–750, https://doi.org/10.1126/science.aat9314, 2018.

Hall, S. J., Weintraub, S. R., Eiriksson, D., Brooks, P. D., Baker, M. A., Bowen, G. J., and Bowling, D. R.: Stream Nitrogen Inputs Reflect Groundwater Across a Snowmelt-Dominated Montane to Urban Watershed, Environmental Science & Technology, 50, 1137–1146, https://doi.org/10.1021/acs.est.5b04805, 2016.

Hammond, J. C. and Kampf, S. K.: Subannual Streamflow Responses to Rainfall and Snowmelt Inputs in Snow-Dominated Watersheds of the Western United States, Water Resources Research, 56, e2019WR026 132, https://doi.org/https://doi.org/10.1029/2019WR026132, 2020.

Hammond, J. C., Sexstone, G. A., Putman, A. L., Barnhart, T. B., Rey, D. M., Driscoll, J. M., Liston, G. E., Rasmussen, K. L., McGrath, D., Fassnacht, S. R., and Kampf, S. K.: High Resolution SnowModel Simulations Reveal Future Elevation-Dependent Snow Loss and Earlier, Flashier Surface Water Input for the Upper Colorado River Basin, Earth's Future, 11, e2022EF003 092, https://doi.org/https://doi.org/10.1029/2022EF003092, 2023.

Hansen, C., Shafiei Shiva, J., McDonald, S., and Nabors, A.: Assessing Retrospective National Water Model Streamflow with Respect to Droughts and Low Flows in the Colorado River Basin, Journal of the American Water Resources Association, 55, 964–975, https://doi.org/https://doi.org/10.1111/1752-1688.12784, 2019.

Harris, I., Osborn, T., Jones, P., and D., L.: Version 4 of the CRU TS monthly high-resolution gridded multivariate climate dataset, Sci Data, 7, https://doi.org/https://doi.org/10.1038/s41597-020-0453-3, 2020.

Haynes, J., Read, A., Chan, A., Martin, D., Regan, R., Henson, W., and Niswonger, R.: Monthly crop irrigation withdrawals and efficiencies by HUC12 watershed for years 2000-2020 within the conterminous United States, https://doi.org/https://doi.org/10.5066/P9LGISUM.

Heike Hofmann, H. W. and Kafadar, K.: Letter-Value Plots: Boxplots for Large Data, Journal of Computational and Graphical Statistics, 26, 469–477, https://doi.org/10.1080/10618600.2017.1305277, 2017.

Hicke, J., Lucatello, S., Mortsch, L., Dawson, J., Aguilar, M. D., Enquist, C., Gilmore, E., Gutzler, D., Harper, S., Holsman, K., Jewett, E., Kohler, T., and Miller, K.: Climate Change 2022: Impacts, Adaptation and Vulnerability. Contribution of Working Group II to the Sixth Assessment Report of the Intergovernmental Panel on Climate Change, chap. 14: North America, p. 1929–2042, Cambridge University Press, Cambridge, UK and New York, NY, USA, https://doi.org/10.1017/9781009325844.016, 2022.

Jasechko, S., Birks, S. J., Gleeson, T., Wada, Y., Fawcett, P. J., Sharp, Z. D., McDonnell, J. J., and Welker, J. M.: The pronounced seasonality of global groundwater recharge, Water Resources Research, 50, 8845–8867, https://doi.org/https://doi.org/10.1002/2014WR015809, 2014.

Jasechko, S., Seybold, H., Perrone, D., Ying, F., and Kirchner, J.: Widespread potential loss of streamflow into underlying aquifers across the USA, Nature, 591, 391–395, https://doi.org/https://doi.org/10.1038/s41586-021-03311-x, 2021.

Ketchum, D., Hoylman, Z., and Huntington, J. e. a.: Irrigation intensification impacts sustainability of streamflow in the Western United States, Commun Earth Environ, 4, 479, https://doi.org/https://doi.org/10.1038/s43247-023-01152-2, 2023.

Kornfield, M.: Rio Grande runs dry in Albuquerque for the first time in 40 years, https://www.washingtonpost.com/climate-environment/2022/07/22/rio-grande-drought/, [Online; posted July 22, 2022, accessed Aug 18, 2022], 2022.

Li, D., Wrzesien, M. L., Durand, M., Adam, J., and Lettenmaier, D. P.: How much runoff originates as snow in the western United States, and how will that change in the future?, Geophysical Research Letters, 44, 6163–6172, https://doi.org/https://doi.org/10.1002/2017GL073551, 2017.

Lin, J., Compton, J. E., Hill, R. A., Herlihy, A. T., Sabo, R. D., Brooks, J. R., Weber, M., Pickard, B., Paulsen, S. G., and Stoddard, J. L.: Context is Everything: Interacting Inputs and Landscape Characteristics Control Stream Nitrogen, Environmental Science & Technology, 55, 7890–7899, https://doi.org/10.1021/acs.est.0c07102, 2021.

McGill, L. M., Brooks, J. R., and Steel, E. A.: Spatiotemporal dynamics of water sources in a mountain river basin inferred through δ^2H and δ^{18}O of water, Hydrological Processes, 35, e14 063, https://doi.org/https://doi.org/10.1002/hyp.14063, 2021.

Miller, M. P., Buto, S. G., Susong, D. D., and Rumsey, C. A.: The importance of base flow in sustaining surface water flow in the Upper Colorado River Basin, Water Resources Research, 52, 3547–3562, https://doi.org/https://doi.org/10.1002/2015WR017963, 2016.

Miller, M. P., Buto, S. G., Lambert, P. M., and Rumsey, C. A.: Enhanced and updated spatially referenced statistical assessment of dissolved-solids load sources and transport in streams of the Upper Colorado River Basin, Tech. rep., US Geological Survey, https://doi.org/https://doi.org/10.3133/sir20175009, 2017.

Miller, O. L., Miller, M. P., Longley, P. C., Alder, J. R., Bearup, L. A., Pruitt, T., Jones, D. K., Putman, A. L., Rumsey, C. A., and McKinney, T.: How will baseflow respond to climate change in the Upper Colorado River Basin?, Geophysical Research Letters, n/a, e2021GL095 085, https://doi.org/https://doi.org/10.1029/2021GL095085, 2021a.

Miller, O. L., Putman, A. L., Alder, J., Miller, M., Jones, D. K., and Wise, D. R.: Changing climate drives future streamflow declines and challenges in meeting water demand across the southwestern United States, Journal of Hydrology X, 11, 100 074, https://doi.org/https://doi.org/10.1016/j.hydroa.2021.100074, 2021b.

Miller, O. L., Putman, A. L., Smith, R. A., Schwarz, G. E., Hess, M. D., McDonnell, M. C., and Jones, D. K.: Temporal variability in irrigated land and climate influences on salinity loading across the Upper Colorado River Basin, 1986-2017, Environmental Research Letters, 19, 024 008, https://doi.org/10.1088/1748-9326/ad18dd, 2024.

Milly, P. and Dunne, K. A.: Colorado River flow dwindles as warming-driven loss of reflective snow energizes evaporation, Science, 367, 1252–1255, https://doi.org/10.1126/science.aay9187, 2020.

Mote, P., Li, S., Lettenmaier, D., Xiao, M., and Engle, R.: Dramatic declines in snowpack in the western U.S., npj Clim Atmos Sci, 1, https://doi.org/https://doi.org/10.1038/s41612-018-0012-1, 2021.

National Oceanographic and Atmospheric Administration: National Water Model CONUS Retrospective Dataset, https://registry.opendata.aws/nwm-archive, data accessed in 2022, 2022.

Nickolas, L. B., Segura, C., and Brooks, J. R.: The influence of lithology on surface water sources, Hydrological Processes, 31, 1913–1925, https://doi.org/https://doi.org/10.1002/hyp.11156, 2017.

Nusbaumer, J., Wong, T. E., Bardeen, C., and Noone, D.: Evaluating hydrological processes in the Community Atmosphere Model Version 5 (CAM5) using stable isotope ratios of water, Journal of Advances in Modeling Earth Systems, 9, 949–977, https://doi.org/https://doi.org/10.1002/2016MS000839, 2017.

Oerter, E., Malone, M., Putman, A., Drits-Esser, D., Stark, L., and Bowen, G.: Every apple has a voice: using stable isotopes to teach about food sourcing and the water cycle, Hydrology and Earth System Sciences, 21, 3799–3810, https://doi.org/10.5194/hess-21-3799-2017, 2017.

Pfahl, S., O'Gorman, P., and Fischer, E.: Understanding the regional pattern of projected future changes in extreme precipitation, Nature Climate Change, 7, 423–427, https://doi.org/https://doi.org/10.1038/nclimate3287, 2017.

Putman, A. L. and Bowen, G. J.: A global database of the stable isotopic ratios of meteoric and terrestrial waters, Hydrology and Earth System Sciences, 23, 4389–4396, https://doi.org/https://doi.org/10.5194/hess-23-4389-2019, 2019.

Putman, A. L., Fiorella, R. P., Bowen, G. J., and Cai, Z.: A global perspective on local meteoric water lines: Meta-analytic insight into fundamental controls and practical constraints, Water Resources Research, 55, 6896–6910, https://doi.org/https://doi.org/10.1029/2019WR025181, 2019.

Putman, A. L., McIlwain, H. E., Rumsey, C. A., and Marston, T. M.: Low flows from drought and water use reduced total dissolved solids fluxes in the Lower Colorado River Basin between 1976 to 2008, Journal of Hydrology: Regional Studies, 52, 101 673, https://doi.org/https://doi.org/10.1016/j.ejrh.2024.101673, 2024.

Ramirez, R.: Great Salt Lake is 'in trouble' as level falls to lowest on record for second year in a row, https://www.cnn.com/2022/07/06/us/great-salt-lake-record-low-climate/index.html, [Online; posted July 6, 2022, accessed Aug 18, 2022], 2022.

Reddy, J., Longley, P. C., McDonnell, M. C., Katoski, M. P., Miller, O. L., and Putman, A.: Hydrogen and oxygen stable isotope mass balance evaluation of the National Water Model (v2.1) streamflow, runoff and groundwater flows, https://doi.org/https://doi.org/10.5066/P9NOD5ES, U.S. Geological Survey data release, 2023.

885 Rubel, F. and Kottek, M.: Observed and projected climate shifts 1901-2100 depicted by world maps of the Köppen-Geiger climate classification, Meteorologische Zeitschrift, 19, 135–141, https://doi.org/10.1127/0941-2948/2010/0430, 2010.

Seabold, S. and Perktold, J.: Statsmodels: Econometric and statistical modeling with python, in: 9th Python in Science Conference, https://conference.scipy.org/proceedings/scipy2010/pdfs/seabold.pdf, 2010.

Seo, B.-C., Krajewski, W. F., and Quintero, F.: Multi-Scale Hydrologic Evaluation of the National Water Model Streamflow Data Assimilation, JAWRA Journal of the American Water Resources Association, 57, 875–884, https://doi.org/https://doi.org/10.1111/1752-1688.12955, 2021.

Siirila-Woodburn, E. R., Rhoades, A. M., Hatchett, B. J., Huning, L. S., Szinai, J., Tague, C., Nico, P. S., Feldman, D. R., Jones, A. D., Collins, W. D., et al.: A low-to-no snow future and its impacts on water resources in the western United States, Nature Reviews Earth & Environment, 2, 800–819, https://doi.org/https://doi.org/10.1038/s43017-021-00219-y, 2021.

895 Solder, J. and Beisner, K.: Critical evaluation of stable isotope mixing end-members for estimating groundwater recharge sources: case study from the South Rim of the Grand Canyon, Arizona, USA, Hydrogeol J, 28, 1575–1591, https://doi.org/https://doi.org/10.1007/s10040-020-02194-y, 2020.

Sprenger, M., Carroll, R. W. H., Marchetti, D., Bern, C., Beria, H., Brown, W., Newman, A., Beutler, C., and Williams, K. H.: Stream water sourcing from high-elevation snowpack inferred from stable isotopes of water: a novel application of d-excess values, Hydrology and Earth System Sciences, 28, 1711–1723, https://doi.org/10.5194/hess-28-1711-2024, 2024.

900 Stets, E. G., Sprague, L. A., Oelsner, G. P., Johnson, H. M., Murphy, J. C., Ryberg, K., Vecchia, A. V., Zuellig, R. E., Falcone, J. A., and Riskin, M. L.: Landscape Drivers of Dynamic Change in Water Quality of U.S. Rivers, Environmental Science & Technology, 54, 4336–4343, https://doi.org/10.1021/acs.est.9b05344, 2020.

The pandas development team: pandas-dev/pandas: Pandas, https://doi.org/10.5281/zenodo.3509134, 2020.

905 Thorslund, J., Bierkens, M., and Oude Essink, G. e. a.: Common irrigation drivers of freshwater salinisation in river basins worldwide, Nature Communications, 12, 4232, https://doi.org/https://doi.org/10.1038/s41467-021-24281-8, 2021.

Towler, E., Foks, S. S., Dugger, A. L., Dickinson, J. E., Essaid, H. I., Gochis, D., Viger, R. J., and Zhang, Y.: Benchmarking high-resolution hydrologic model performance of long-term retrospective streamflow simulations in the contiguous United States, Hydrology and Earth System Sciences, 27, 1809–1825, https://doi.org/10.5194/hess-27-1809-2023, 2023.

910 Tulley-Cordova, C. L., Putman, A. L., and Bowen, G. J.: Stable Isotopes in Precipitation and Meteoric Water: Sourcing and Tracing the North American Monsoon in Arizona, New Mexico, and Utah, Water Resources Research, 57, e2021WR030 039, https://doi.org/https://doi.org/10.1029/2021WR030039, 2021.

University of East Anglia Climatic Research Unit and Harris, I.C. and Jones, P.D. and Osborn, T. : CRU TS4.05: Climatic Research Unit (CRU) Time-Series (TS) version 4.05 of high-resolution gridded data of month-by-month variation in climate (Jan. 1901- Dec. 2020),
915 https://catalogue.ceda.ac.uk/uuid/c26a65020a5e4b80b20018f148556681, accessed January, 2022, 2021.

U.S. Environmental Protection Agency: National lakes assessment: A collaborative survey of the nations's lakes, Tech. rep., Office of Water and Office of Research and Development, https://www.epa.gov/sites/default/files/2013-11/documents/nla_newlowres_fullrpt.pdf, 2009.

U.S. Environmental Protection Agency: National Lakes Assessment 2012: A Collaborative Survey of Lakes in the United States, Tech. rep., Office of Water and Office of Research and Development, https://www.epa.gov/sites/default/files/2016-12/documents/nla_report_dec_2016.pdf, 2016a.

U.S. Environmental Protection Agency: National rivers and streams assessment 2008-2009: A collaborative survey, Tech. rep., Office of Water and Office of Research and Development, https://www.epa.gov/sites/default/files/2016-03/documents/nrsa_0809_march_2_final.pdf, 2016b.

U.S. Environmental Protection Agency: National rivers and streams assessment 2013-2014: A collaborative survey, Tech. rep., Office of Water and Office of Research and Development, https://www.epa.gov/system/files/documents/2021-10/nrsa_13-14_report_508_ci_2021-10-15.pdf, 2020.

U.S. Geological Survey: National Hydrography Dataset (ver. 2.1), https://www.usgs.gov/national-hydrography/access-national-hydrography-products, accessed Oct, 2021, 2019.

U.S. Geological Survey: National Water Information System: U.S. Geological Survey web interface, https://doi.org/http://dx.doi.org/10.5066/F7P55KJN, 2022.

U.S. Geological Survey, National Geospatial Technical Operations Center: Watershed Boundary Dataset (WBD) - USGS National Map Downloadable Data Collection, https://www.sciencebase.gov/catalog/item/51361e87e4b03b8ec4025c22#:~:text=Citation,Data%20Collection%3A%20U.S.%20Geological%20Survey., scienceBase Data Release, 2023.

Wes McKinney: Data Structures for Statistical Computing in Python, in: Proceedings of the 9th Python in Science Conference, edited by Stéfan van der Walt and Jarrod Millman, pp. 56 – 61, https://doi.org/10.25080/Majora-92bf1922-00a, 2010.

Williams, A., Cook, B., and Smerdon, J.: Rapid intensification of the emerging southwestern North American megadrought in 2020–2021, Nat. Clim. Chang., 12, https://doi.org/https://doi.org/10.1038/s41558-022-01290-z, 2022.

Windler, G., Brooks, J. R., Johnson, H. M., Comeleo, R. L., Coulombe, R., and Bowen, G. J.: Climate Impacts on Source Contributions and Evaporation to Flow in the Snake River Basin Using Surface Water Isoscapes (δ^2H and δ^{18}O), Water Resources Research, 57, e2020WR029 157, https://doi.org/https://doi.org/10.1029/2020WR029157, 2021.

Wolf, M. A., Jamison, L. R., Solomon, D. K., Strong, C., and Brooks, P. D.: Multi-Year Controls on Groundwater Storage in Seasonally Snow-Covered Headwater Catchments, Water Resources Research, 59, e2022WR033 394, https://doi.org/https://doi.org/10.1029/2022WR033394, 2023.

Xia, C., Liu, Y., Meng, Y., Liu, G., Huang, X., Chen, Y., and Chen, K.: Stable isotopes reveal the surface water-groundwater interaction and variation in young water fraction in an urbanized river zone, Urban Climate, 51, 101 641, https://doi.org/https://doi.org/10.1016/j.uclim.2023.101641, 2023.

Yang, Z., Qian, Y., Liu, Y., Berg, L. K., Hu, H., Dominguez, F., Yang, B., Feng, Z., Gustafson Jr, W. I., Huang, M., and Tang, Q.: Irrigation Impact on Water and Energy Cycle During Dry Years Over the United States Using Convection-Permitting WRF and a Dynamical Recycling Model, Journal of Geophysical Research: Atmospheres, 124, 11 220–11 241, https://doi.org/https://doi.org/10.1029/2019JD030524, 2019.